TU Delft

Delft University of Technology

Document Version
Final published version

Licence
CC BY

Citation (APA)
Hadi, A., Pang, Y., Adema, A., van der Stel, J., & Schott, D. (2026). Industrial-scale DEM modelling of segregation in the blast furnace charging system. *Powder Technology*, *471*, Article 122116. https://doi.org/10.1016/j.powtec.2026.122116

Important note
To cite this publication, please use the final published version (if applicable).
Please check the document version above.

Copyright
In case the licence states “Dutch Copyright Act (Article 25fa)”, this publication was made available Green Open Access via the TU Delft Institutional Repository pursuant to Dutch Copyright Act (Article 25fa, the Taverne amendment). This provision does not affect copyright ownership.
Unless copyright is transferred by contract or statute, it remains with the copyright holder.

Sharing and reuse
Other than for strictly personal use, it is not permitted to download, forward or distribute the text or part of it, without the consent of the author(s) and/or copyright holder(s), unless the work is under an open content license such as Creative Commons.

Takedown policy
Please contact us and provide details if you believe this document breaches copyrights.
We will remove access to the work immediately and investigate your claim.

This work is downloaded from Delft University of Technology.

Powder Technology 471 (2026) 122116

Contents lists available at ScienceDirect

Powder Technology

journal homepage: www.journals.elsevier.com/powder-technology

Industrial-scale DEM modelling of segregation in the blast furnace charging system

Ahmed Hadi [a],*, Yusong Pang [a], Allert Adema [b], Jan van der Stel [b], Dingena Schott [a]

[a] Department of Maritime and Transport Technology, Faculty of Mechanical Engineering, Delft University of Technology, Delft, 2628CD, The Netherlands
[b] Tata Steel Netherlands, Wenckebachstraat 1, Velsen-Noord, 1951 HL, The Netherlands

GRAPHICAL ABSTRACT

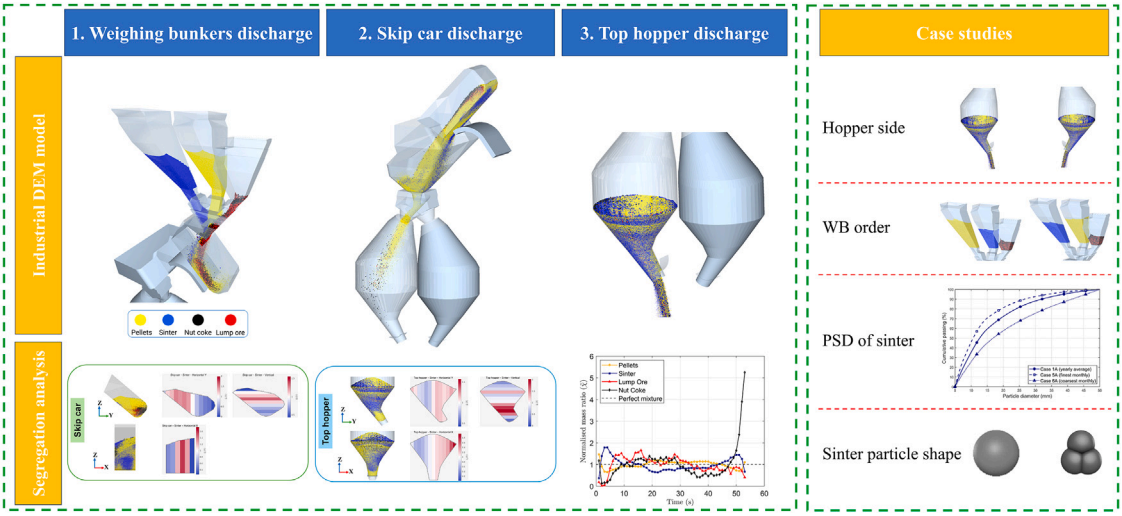

HIGHLIGHTS

- Industrial-scale DEM applied to blast furnace charging system.
- Segregation of the ferrous mixture analysed under real conditions.
- Segregation generally decreases from skip car to top hopper.
- Lump ore and nut coke segregate strongly; pellets segregate least.
- Bunker order strongly affects segregation; PSD and shape effects are relatively minor.

ARTICLE INFO

Keywords:
Discrete element method (DEM)
Segregation
Blast furnace
Hopper

ABSTRACT

Segregation of the ferrous burden during blast furnace (BF) charging can cause uneven layer formation at the furnace throat, reducing bed permeability and disrupting gas–solid interaction. This study applies a discrete element method (DEM) model to the industrial-scale BF charging system (from the skip car to top hopper discharge) to examine segregation under real operating conditions. The model includes the full ferrous mixture (pellets, sinter, lump ore, and nut coke) and the real-scale geometries. A reference case representing current

* Corresponding author.
E-mail address: a.h.hadi-1@tudelft.nl (A. Hadi).

https://doi.org/10.1016/j.powtec.2026.122116
Received 29 September 2025; Received in revised form 29 December 2025; Accepted 4 January 2026
Available online 8 January 2026
0032-5910/© 2026 The Author(s). Published by Elsevier B.V. This is an open access article under the CC BY license (http://creativecommons.org/licenses/by/4.0/).

Industrial-scale modelling

practice is analysed in detail and compared with systematically varied case studies. The results show that segregation generally decreases from the skip car to the top hopper due to partial remixing, but strong segregation is still observed. Lump ore and nut coke exhibit the strongest segregation, while pellets remain the least segregated. The order of pellets and sinter in the weighing bunkers strongly influences their segregation patterns, whereas variations in the sinter particle size distribution (PSD) and particle shape have only limited effects. The insights from this study provide a basis for developing practical strategies to mitigate segregation in industrial BF charging.

1. Introduction

In blast furnace, segregation can adversely affect the distribution of materials on the burden surface, which in turn has a detrimental effect on bed permeability [1]. This affected permeability leads to inconsistencies in pressure drop, causing inefficient use of reductant gas and resulting in both economic and environmental consequences [2]. Therefore, it is crucial to investigate and understand segregation within the blast furnace processes.

Conducting in-situ measurements of segregation within the blast furnace charging system is both costly and impractical because of the large-scale equipment and harsh operating environment. To overcome these challenges, several lab-scale experimental studies have been carried out to examine segregation and burden distribution under controlled conditions [3–6]. For instance, Spence [3] reported that the segregation patterns observed during hopper discharge are closely linked to those formed during the filling of the receiving hopper. Also, Mio et al. [4] observed delayed discharge of coarser sinter particles in a 1/3-scale furnace experiment, indicating size segregation within both the surge and parallel hoppers. Although these studies provided valuable insights into the overall segregation behaviour, they fail to capture the particle-scale mechanisms responsible for the observed trends. To address this limitation, DEM can be employed as a physics-based modelling approach to gain detailed insight into segregation phenomena within the blast furnace.

Many DEM studies have investigated the segregation and distribution of materials in blast furnace charging systems [1,7–38]. However, a large proportion of these works have focused on the region after the top hopper, particularly chute flow and burden surface distribution at the blast furnace throat [8,19,39,40]. Fewer studies have explicitly examined the upstream stages of the charging system, where segregation already begins to develop [14,23,35,37].

Many previous studies also considered only one or two burden materials at a time, and only a few have attempted to model the complete ferrous burden [22,26,31–38,40]. Furthermore, the DEM input parameters in these works were typically taken directly from the literature, rather than being calibrated for the specific ore types under investigation. In addition, the focus has primarily been on size segregation within individual material types such as pellets, sinter or coke, with only a limited number of studies addressing the more complex case of multi-component segregation [40,42].

In our earlier work [43], we modelled a mixture of pellets and sinter in an industrial-scale charging configuration using literature-based DEM parameters. While that study provided valuable initial insights, including the observation that upstream mixing strongly influences downstream segregation, its simplified scope highlighted the need for a more complete and realistic modelling approach.

In the present study, we build on earlier DEM investigations by modelling the multi-component segregation in the blast furnace charging process using the actual plant geometry and operating conditions of the charging system at Tata Steel IJmuiden, covering the full sequence from the weighing bunkers to top-hopper discharge. While individual modelling aspects, such as multi-component segregation, calibrated material parameters, simulating the full charging process, and the use of actual plant geometry, have each been considered in prior studies, they have rarely been examined jointly within a single calibrated and industrially realistic framework. The DEM model, previously calibrated against laboratory experiments for pellet–sinter mixtures [44], is here extended to represent the full ferrous burden (pellets, sinter, lump ore and nut coke) and to incorporate realistic particle size distributions and operational settings. This enables a realistic evaluation of both material-related factors (e.g. PSD variation, particle shape and lump ore type) and operational factors (e.g. weighing-bunker order, hopper side and wall friction) on segregation behaviour.

In this way, the study complements existing DEM studies on material distribution in BF [1,8–38] by providing an integrated assessment of multi-component segregation throughout the upstream charging process, rather than focusing on individual materials, isolated process stages, or down-scaled geometries. The main objectives are (i) to identify the root causes of multi-component segregation within the charging system and (ii) to systematically evaluate the influence of material properties, particle characteristics and operational factors on segregation behaviour through a series of case studies.

This paper is structured as follows. Section 2 presents the DEM modelling framework, including the model setup, geometries, and the approach used to quantify segregation. Section 3 introduces the defined case studies, discusses the results of the reference case in detail, and compares the outcomes of the remaining cases against this baseline. Finally, Section 4 summarises the key findings of this study.

2. Materials and methods

2.1. Discrete element method

DEM simulations were carried out using the Hertz-Mindlin (no-slip) contact model [45], combined with an elastic–plastic spring–dashpot rolling friction model (referred to as type C in Ai et al. [46]), as described in our previous paper [47]. All simulations were performed using the commercial software EDEM v2024.1 and were executed on the DelftBlue supercomputing cluster [48]

2.2. Simulation configuration

2.2.1. Materials and DEM parameters

The ferrous mixture used in the blast furnace charging system is modelled to reflect industrial practice. As illustrated in Fig. 1, this mixture mainly consists of pellets, sinter, and lump ore. In certain operations, including at Tata Steel IJmuiden, a small proportion of nut coke (i.e., fine-sized coke) is also introduced into the ferrous mixture to increase the productivity.

For pellets and sinter, the calibrated DEM parameters from our previous paper were employed to ensure an accurate representation of the flow behaviour [44]. For lump ore and nut coke, where direct calibration was not conducted, the DEM parameters were adopted from the study by [8], which investigated similar materials under comparable conditions. For interactions between different material types (e.g., pellet–sinter or pellet–lump ore), the inter-material contact parameters were estimated as the average of the corresponding values for the two interacting materials, as proved to be accurate in our previous study [44].

The realistic size distributions of all materials, as used in Tata Steel's operations, were implemented in the simulations, as shown in Fig. 2. The detailed PSD of all materials is presented Table A.3 in Appendix.

Fig. 1. The main components of the ferrous mixture: sinter (left), pellets (middle), and lump ore (right) [41].

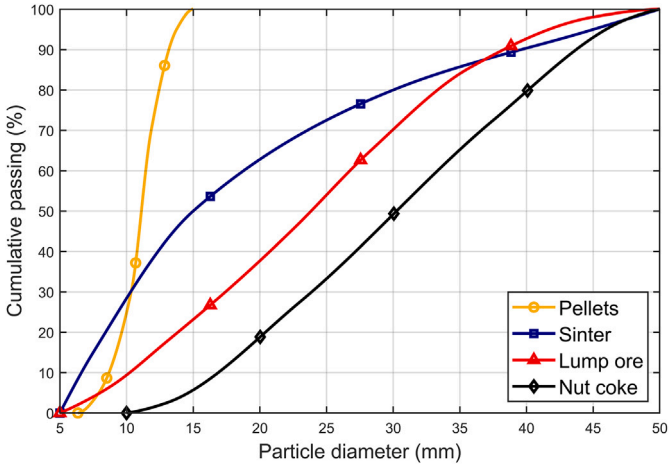

Fig. 2. Particle size distribution of the materials used in this study.

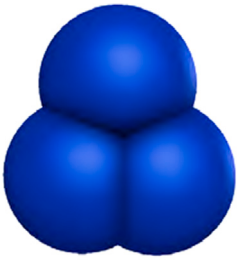

Fig. 3. The clumped spheres model used to simulate sinter particles in the corresponding case study (sphericity = 0.878).

To improve computational efficiency, the particle size was scaled by a factor of two, which reduced the simulation time by roughly a factor of 16 while still maintaining accurate segregation predictions, as shown in our previous work [43]. Moreover, to keep computational costs manageable, spherical particles were used to represent particle shapes in the simulations. However, in one specific case study, non-spherical particles, illustrated in Fig. 3, were employed to investigate the effect of explicitly modelling the irregular shape of sinter particles on flow and segregation behaviour. This particle shape has been successfully calibrated and validated for sinter particles in our previous work [44]. A comprehensive list of all DEM parameters used is provided in Table A.4 in Appendix.

2.2.2. Geometries and the charging process

Fig. 4 illustrates the simulation geometry used in this study to model the blast furnace charging system at Tata Steel IJmuiden. The system contains three weighing bunkers (WBs), designated for storing pellets, sinter, and a mixture of lump ore and nut coke, respectively. During each charging cycle, approximately 20 tonnes of pellets, 12 tonnes of sinter, 2.4 tonnes of lump ore, and 0.75 tonnes of nut coke are loaded into the corresponding bunkers.

The outlets of the pellet and sinter WBs are opened simultaneously in a controlled manner to ensure that both materials are emptied at the same time. In contrast, the outlet of the lump ore/nut coke bunker is opened fully and it is emptied instantly (Fig. 5(a)).

In the actual industrial process, the filled skip car moves up along an inclined rail before discharging the materials. However, since this upward movement is not expected to induce any significant material segregation, it was excluded from the simulation for computational efficiency. Therefore, the skip car was directly positioned at the top discharge point (* in Fig. 4), where it begins to tilt.

Upon tilting, the ferrous mixture is discharged into the receiving funnel and then flows through a series of components, including a semi-cylindrical chute at the diverter gate, before being deposited into one of the top hoppers (Fig. 5(b)). This entire charging sequence is then repeated for the second skip car to complete a full batch cycle. Finally, the valve of the top hopper is opened (Fig. 5(c)), allowing the ferrous material to discharge. The mixture then enters the lower funnel and pass through the rotating chute, before being deposited at the furnace throat.

2.3. Quantifying segregation

Segregation was measured at three key locations: within the skip car, within the top hopper (after both skip cars are loaded), and after the discharge from the top hopper. The approach used to quantify segregation at these locations is described below.

2.3.1. Segregation in the skip car and top hopper

The relative standard deviation (RSD), a grid-dependent segregation index, was used to quantify segregation in both the skip car and the top hoppers. The procedure for calculating RSD is explained in detail in our previous work [47]. An RSD value of zero corresponds to a perfectly homogeneous mixture, whereas higher RSD values indicate a greater degree of segregation.

Since segregation can occur in different spatial directions, namely horizontal, vertical, and throughout the full volume, RSD was calculated separately for each of these directions. Furthermore, because the segregation behaviour may vary across different material types, the RSD was also computed individually for each material (i.e., pellets, sinter, lump ore, and nut coke).

As the RSD is a grid-dependent segregation index, selecting an appropriate bin size is crucial for meaningful comparison across materials and directions. To maintain a physically relevant resolution, the bin size was defined as ten times the mean particle size (based on the median diameters, D_{50}, of all materials).

$$b = 10\,\bar{D}_{50}, \qquad \bar{D}_{50} = \frac{1}{N_m}\sum_{i=1}^{N_m} D_{50,i}, \tag{1}$$

where N_m is the number of material types ($N_m = 4$). The number of bins k_j in each spatial direction j ($j = x, y, z$) was then obtained as

$$k_j = \left\lfloor \frac{L_j}{b} \right\rfloor, \tag{2}$$

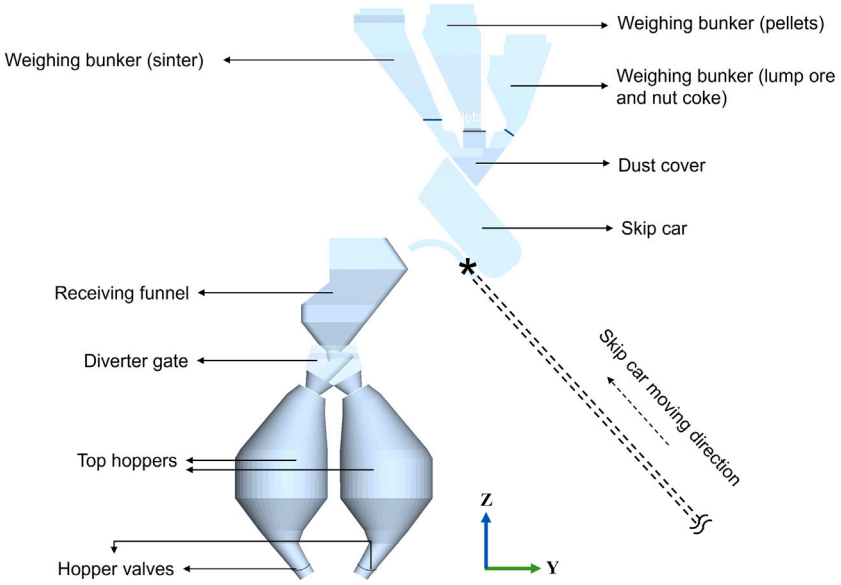

Fig. 4. The geometry model used in this study. For practical reasons, the WBs and the skip car are placed at the location (*), while in practice, they are located at the bottom, and the skip car moves up in the mentioned direction.

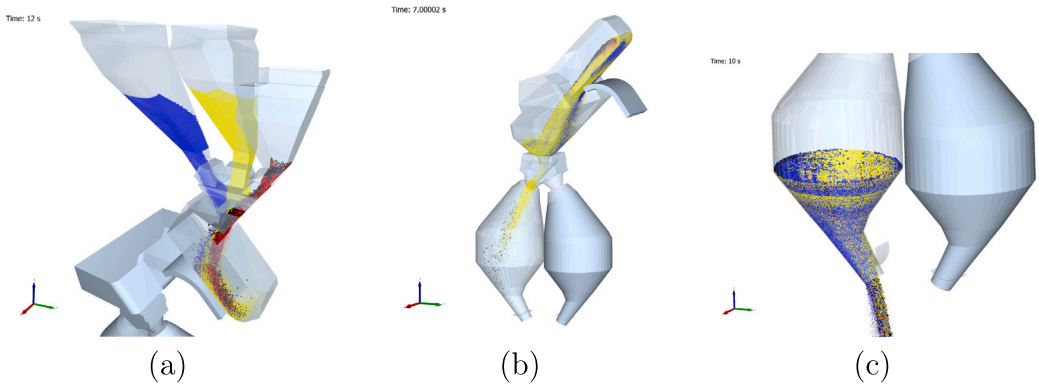

Fig. 5. Snapshots of the DEM simulation showing the charging sequence: (a) discharge of weighing bunkers into the skip car, (b) discharge of the skip car into the receiving funnel, and (c) discharge of the top hopper. The particle colours are consistent in all simulations: pellets (yellow), sinter (blue), lump ore (red), and nut coke (black).

with L_j being the domain length in direction j. This definition ensures that the grid resolution scales consistently with the characteristic particle size, enabling direct comparison of RSD values among materials with different size distributions.

To complement the RSD analysis and gain insights into the local distribution of the materials, the normalised mass ratio (NMR), $\tilde{\chi}_i(k_j)$, was also calculated for material i in the kth bin in j direction:

$$\tilde{\chi}_i(k_j) = \frac{\chi_i(k_j)}{\chi_i^0} \tag{3}$$

where $\chi_i(k_j)$ is the local mass ratio of material i in bin k in j direction, and χ_i^0 is its initial mass ratio in the system (e.g., skip car). A value of $\tilde{\chi}_i(k_j) = 1$ indicates that the local proportion of material i matches the initial bulk proportion; $\tilde{\chi}_i(k_j) > 1$ indicates over-representation, and $\tilde{\chi}_i(k_j) < 1$ indicates under-representation. An example of the NMR representation is shown in Fig. 6, illustrating the material distribution in both the skip car and the top hopper. For each geometry, the y–z view is used to present the NMR in the vertical and horizontal (y) directions, while the x–z view is used to present the NMR in the horizontal (x) direction.

It is important to note that the particle size distributions differ across materials, and using a uniform bin size based on a single particle type could bias the RSD calculation. To ensure consistency and comparability across materials, the bin size was set to 10 times a reference particle diameter (through a sensitivity analysis of the bin size effect), d_{ref}, calculated as the mean of the median diameters (D_{50}) of all materials. This approach provides a representative sampling resolution relative to the overall particle size range in the mixture.

2.3.2. Segregation after discharging the top hopper

Unlike the other two regions within the skip car and top hopper, where a static measurement of segregation is possible, segregation after hopper discharge is dynamic and measured over time during the discharge process. To enable the measurement, a cylindrical sampling volume was defined just below the hopper outlet, as shown in Fig. 7. This region captures the mixture of materials exiting the hopper and allows for time-resolved segregation analysis. During the discharge process, the mass of each material (i.e., pellets, sinter, lump ore, and nut coke) within the sampling volume was recorded at 1-second intervals during a total discharging time of roughly 50 s.

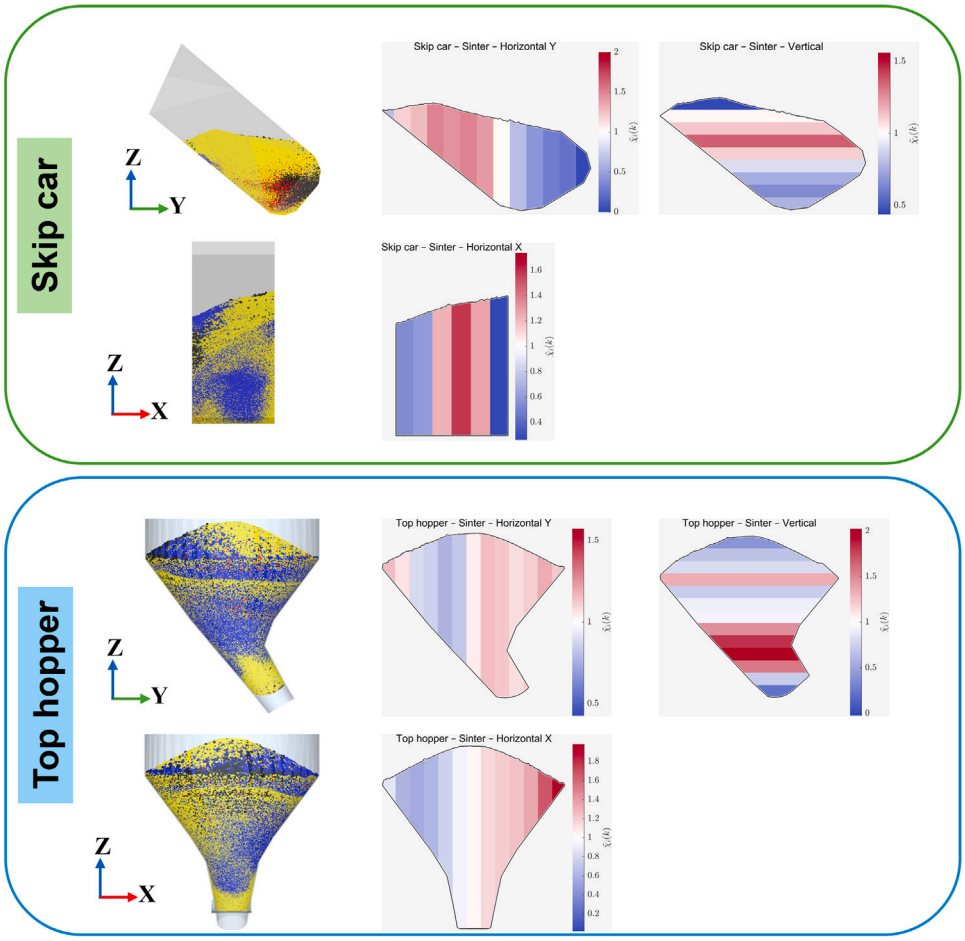

Fig. 6. An example of the normalised mass ratio (NMR) for sinter in the skip car (top) and top hopper (bottom), shown in the horizontal (x and y) and vertical (z) directions, alongside the corresponding views of the geometries. The coordinate system is Cartesian, where the z-axis represents the vertical direction (aligned with gravity), and the x and y axes correspond to two perpendicular horizontal directions, representing longitudinal cross-sections of the geometry.

At each recorded time step t, the instantaneous mass ratio of material i was computed by dividing its mass by the total mass of all materials within the sampling volume:

$$\chi_i(t) = \frac{m_i(t)}{\sum_{j=1}^{n} m_j(t)} \tag{4}$$

where $\chi_i(t)$ is the mass ratio of material i at time t, $m_i(t)$ is the mass of material i at time t within the cylindrical sampling space, calculated by summing the individual particle masses of material i whose centroids lie inside this region, and n is the total number of material types (i.e., 4: pellets, sinter, lump ore, and nut coke).

To assess segregation over time, the normalised mass ratio was then calculated by comparing the instantaneous value to the initial mass fraction of that material in the hopper:

$$\tilde{\chi}_i(t) = \frac{\chi_i(t)}{\chi_i^0} \tag{5}$$

where $\tilde{\chi}_i(t)$ is the normalised mass ratio (NMR) of material i at time t, and χ_i^0 is the initial mass ratio of material i, based on the total mass loaded into the top hopper.

This formulation is similar to Eq. (3), with the distinction that here the sampling is performed over time rather than across spatial bins. Similarly, in an ideally mixed system, $\tilde{\chi}_i(t)$ remains constant at 1 throughout the discharge period. Any deviation from this value indicate segregation:

- $\tilde{\chi}_i(t) > 1$: the material is over-represented at time t
- $\tilde{\chi}_i(t) < 1$: the material is under-represented at time t

To visualise these dynamics, time series of $\tilde{\chi}_i(t)$ were plotted for each material, with a reference line at $\tilde{\chi}_i = 1$ indicating perfect mixing, as illustrated in Fig. 8. To ensure the reliability of the results, a threshold filter was applied: only time steps where the total mass in the sampling volume exceeded 50 kg were considered. This step minimised numerical artefacts that can arise during the early stages of discharge when mass flow is low.

3. Results and discussion

In this section, the segregation behaviour is analysed in detail for the reference case, followed by a comparison with the defined case studies. The analysis focuses on segregation at various stages of the charging process, from the skip car to the top hopper discharge, as mentioned in Section 2.3.

3.1. Definition of case studies

A total of nine case studies were defined to investigate the influence of operational, material, and particle-related factors on segregation during the BF charging process. The cases are summarised in Table 1. Two distinct reference cases were used: Case 1, based on the initial

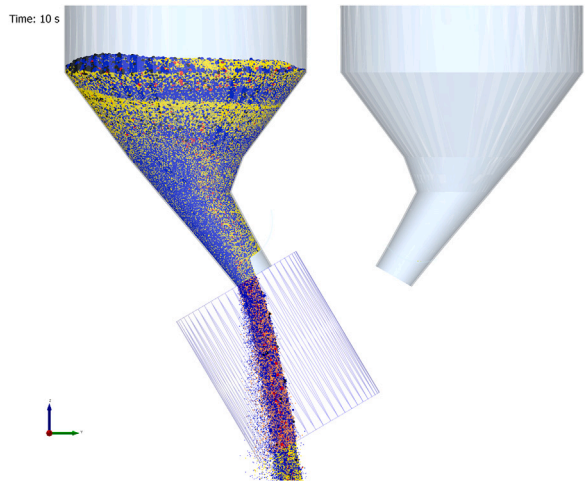

Fig. 7. The cylindrical sampling volume used to measure the mass ratio of each material at each time step during top hopper discharge.

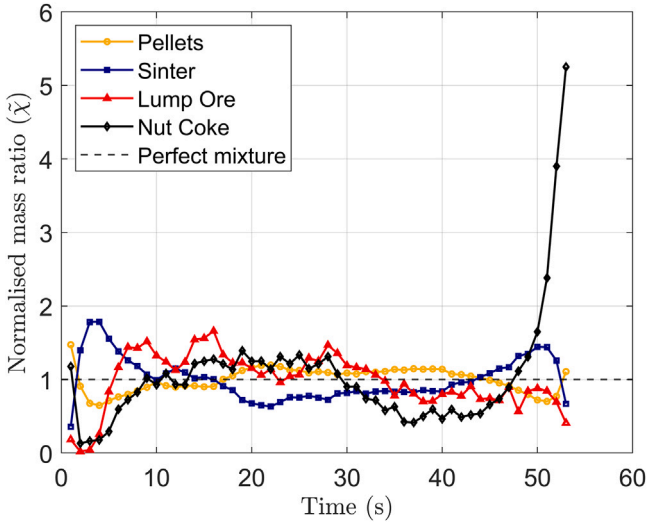

Fig. 8. Example plot showing the segregation behaviour of different materials during top hopper discharge, based on their normalised mass ratios (NMR) over time. The dashed line represents a perfectly mixed state.

PSD data, served as the baseline for operational and material variations (Cases 2, 3, 4, 7, and 8), while Case 1A, defined using updated plant data from Tata Steel for sinter PSD, served as the baseline for the PSD sensitivity study (Cases 5A and 6A). The variations examined include hopper-side asymmetry (Case 2), reversing the order of pellets and sinter in the weighing bunkers (Case 3), reduced particle–wall sliding friction (Case 4), variability in sinter PSD with finer (Case 5A) and coarser (Case 6A) distributions, an alternative lump ore type (Case 7), and the use of non-spherical (clumped) particles for sinter (Case 8). In all cases, only one parameter was varied relative to the reference, enabling the isolated assessment of its effect on segregation.

In the following subsections, the results of the reference case are presented, followed by comparisons with the other cases. To make these comparisons quantitative, the relative difference in RSD between each case and the reference (Case 1) was calculated as:

$$\Delta\mathrm{RSD} = \frac{\mathrm{RSDcase} - \mathrm{RSDref}}{\mathrm{RSD}_{\mathrm{ref}}} \tag{6}$$

ΔRSD expresses how much segregation in a given case increases or decreases relative to the reference. For clarity and a quick overview, Fig. 9 provides an example of the visualisation method: results for different materials, directions, and locations are colour-coded, with blue indicating lower segregation and red indicating higher segregation compared to the reference case.

3.2. Reference case (Case 1)

In this section, the segregation behaviour is analysed in detail for the reference case (Case 1). Segregation is evaluated at three key stages of the charging process: within the skip car, within the top hopper, and after discharging from the top hopper.

Before proceeding with the analysis, it is important that the necessity of repeating the simulations be assessed to account for potential variability. To investigate this, the first step of the process, i.e., the discharge of materials from the weighing bunkers into the skip car, was simulated three times. This approach allowed the evaluation of the variability in the segregation measurements across different spatial directions and for each material.

Table 2 presents the results of the three simulation repetitions. The last column shows the coefficient of variation (CoV) of the RSD values across the repetitions, expressed as a percentage, and calculated as $\mathrm{CoV}\ (\%) = \frac{\sigma_{\mathrm{RSD}}}{\mu_{\mathrm{RSD}}} \times 100$, where σ_{RSD} and μ_{RSD} are the standard deviation and mean of the RSD values, respectively. CoV reflects the degree of variability in the segregation results due to the stochastic nature of the simulations. As shown in the table, the CoV values are consistently low for all materials and directions, showing very low variability. Therefore, repeating the simulations was deemed unnecessary for the rest of this study.

3.2.1. Segregation in the skip car and top hopper

Fig. 10 presents the RSD values for all four materials (pellets, sinter, lump ore, and nut coke) within the skip car and top hopper, across different spatial directions. Overall, segregation decreases from the skip car to the top hopper, indicating a degree of remixing during flowing through the receiving funnel. However, an exception is observed for vertical segregation of pellets and sinter, which increases slightly in the top hopper. This may be attributed to the fact that two skip cars are loaded into the top hopper, creating a vertically layered structure where the material from the second skip car is deposited on top of the first. Such sequential filling can increase vertical compositional differences, resulting in higher RSD in the vertical direction.

Pellets and sinter show relatively low RSD values compared to lump ore and nut coke, with sinter showing slightly higher segregation than pellets. For both pellets and sinter, segregation occurs mostly in the horizontal directions, particularly along the x-axis. To investigate this further, the NMR of pellets and sinter in the x-direction within the skip car were examined, as shown in Fig. 11.

The results clearly show that pellets and sinter are not uniformly distributed in the x-direction of the skip car. For pellets (Fig. 11(a)), higher concentrations are observed on the left side of the skip car, whereas sinter (Fig. 11(b)) is more concentrated in the central region. This spatial bias is mainly the result of insufficient mixing of the materials during discharging from the weighing hoppers, as also noted in our preliminary study [43]. In particular, the observed segregation in the x-direction can be linked to the configuration of the weighing hoppers and the presence of the dust cover. The asymmetric positioning and geometry of the weighing bunkers likely promote uneven loading, resulting in the discharge of certain materials into specific areas of the skip car.

In contrast to pellets and sinter, Fig. 10 indicates that lump ore and nut coke have substantially higher segregation. This behaviour is mainly due to their relatively smaller total mass, which results in their discharge from the weighing bunker being completed much more quickly than for pellets and sinter. Consequently, they concentrate in specific regions of the skip car, as illustrated in Fig. 12(a). In addition, nut coke is observed to segregate from lump ore. This separation arises

Table 1
Summary of the nine case studies. Case 1 is the reference for Cases 2, 3, 4, 7, and 8, while Case 1A is the reference for the PSD sensitivity analysis of sinter (5A and 6A). The highlighted cells indicate the factors that vary from the corresponding reference case.

Case	Hopper Side	WB Order	Wall Friction	PSD of Sinter	Lump Ore Type	Sinter Shape
Case 1 (Ref)	Left	Normal	WF	Avg	A, B	Spherical
Case 1A	Left	Normal	WF	Avg (updated)	A, B	Spherical
Case 2	Right	Normal	WF	Avg	A, B	Spherical
Case 3	Left	Reversed	WF	Avg	A, B	Spherical
Case 4	Left	Normal	WF –25%	Avg	A, B	Spherical
Case 5A	Left	Normal	WF	Min	A, B	Spherical
Case 6A	Left	Normal	WF	Max	A, B	Spherical
Case 7	Left	Normal	WF	Avg	C	Spherical
Case 8	Left	Normal	WF	Avg	A, B	Non-spherical

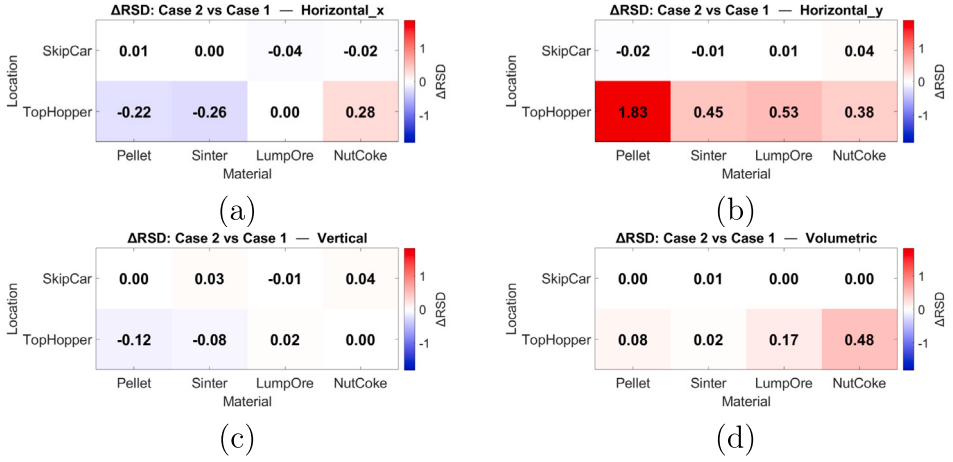

Fig. 9. Illustration of the relative difference in RSD (ΔRSD) between a given case (e.g., Case 2) and the reference case (Case 1), shown for: (a) Horizontal (X), (b) Horizontal (Y), (c) Vertical (Z), and (d) Volumetric directions.

Table 2
RSD values from three simulation repetitions (Rep1–Rep3) for different materials and directions within the skip car, along with the coefficient of variation (CoV) of the RSD values (expressed in percentage) to quantify variability across repetitions.

Direction	Material	Rep1	Rep2	Rep3	CoV (%)
Vertical	Pellet	0.134	0.129	0.130	1.6
	Sinter	0.244	0.250	0.248	1.0
	LumpOre	1.246	1.220	1.239	0.9
	NutCoke	1.136	1.156	1.144	0.7
Horizontal (X)	Pellet	0.257	0.260	0.257	0.5
	Sinter	0.572	0.576	0.565	1.0
	LumpOre	0.527	0.517	0.495	2.6
	NutCoke	0.661	0.656	0.653	0.6
Horizontal (Y)	Pellet	0.197	0.194	0.202	2.1
	Sinter	0.508	0.505	0.507	0.2
	LumpOre	1.119	1.133	1.140	0.9
	NutCoke	0.895	0.943	0.962	3.2
Volumetric	Pellet	0.513	0.516	0.512	0.3
	Sinter	1.017	1.028	1.018	0.5
	LumpOre	2.115	2.103	2.113	0.2
	NutCoke	2.697	2.810	2.808	1.9

from their density difference, whereby buoyancy-driven segregation causes the heavier lump ore particles to sink deeper into the mixture.

Since lump ore and nut coke are mostly deposited near the bottom of the skip car (see Fig. 12(a)), they are discharged last when the skip car tilts, ultimately ending up on the surface of the mixture in the receiving funnel, as illustrated in Fig. 12(b). This sequence results in a layer of lump ore and nut coke forming at the top of the mixture in the top hopper, which contributes to their sustained high vertical segregation. Fig. 13 shows the distribution of lump ore and nut coke in the top hopper after the first and second skip car loads.

Another observation from Fig. 13 is that most of the nut coke tends to move towards the left-hand wall of the hopper during discharge. This behaviour occurs because lump ore, with a higher particle density and slightly smaller particle size, tends to deposit and remain closer to the discharge point. Consequently, this promotes greater horizontal segregation in the x-direction of the top hopper for nut coke, as shown in Fig. 10(d).

It should be noted that the RSD values measured with volumetric bin systems are inherently higher than those calculated for a single direction, as the smaller bin size in the volumetric scheme increases sensitivity to local composition variations. When considering these volumetric RSD values, which capture segregation across all three spatial dimensions, it becomes clear that all materials remain notably segregated, with nut coke exhibiting the highest overall RSD. This indicates that the current charging configuration does not promote effective mixing, even after the material is transferred through the receiving funnel.

3.2.2. *Segregation after discharging the top hopper*

Regarding segregation during the discharge of the top hopper, Fig. 14 shows the temporal evolution of the NMR for each material (see Eq. (5)). After an initial discharging period, pellets show a relatively stable discharge profile, whereas sinter and lump ore display moderate fluctuations throughout the process. In contrast, nut coke demonstrates the most pronounced segregation, with its mass ratio rising sharply in the final discharge stage (50–55 s) to more than five times its initial mass ratio within the mixture.

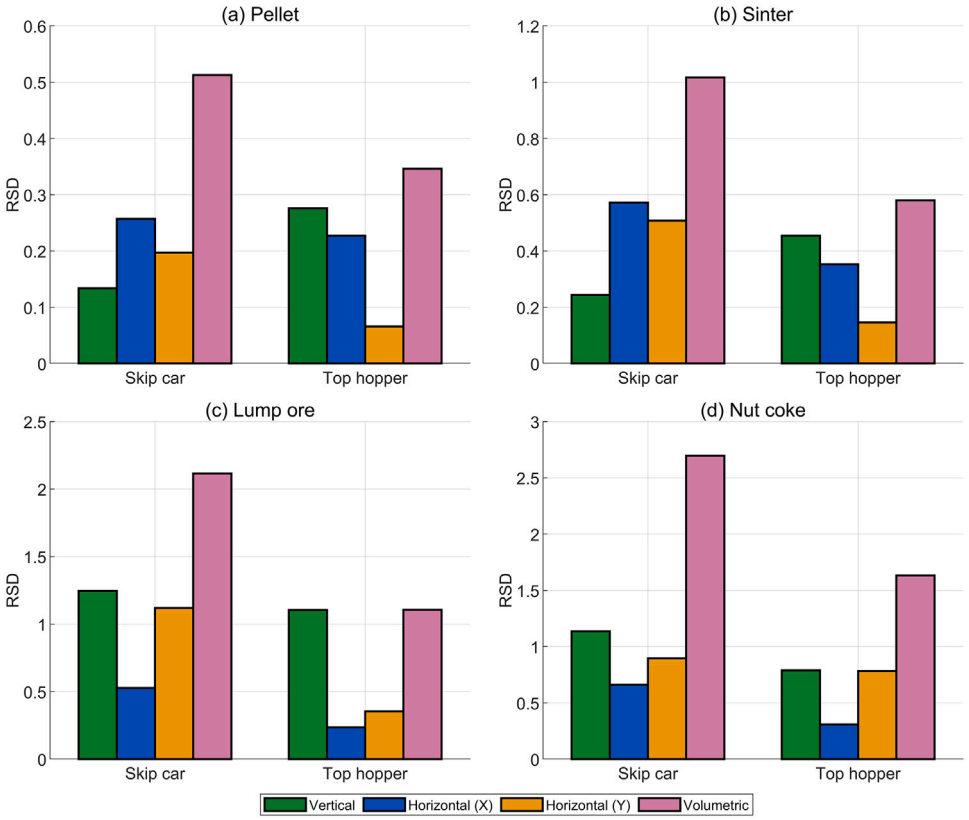

Fig. 10. RSD values for (a) pellets, (b) sinter, (c) lump ore, and (d) nut coke, measured in different directions within the skip car and the top hopper.

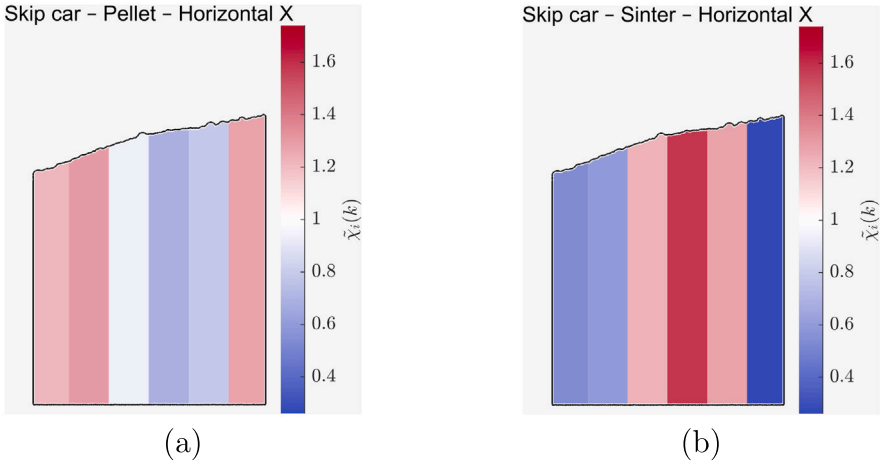

Fig. 11. NMR in the x-direction within the skip car for: (a) pellets, and (b) sinter.

The whole discharge time can be divided into some regions with different segregation behaviour, as described below.

- **1–9 seconds:** In the initial stage of discharge, all four materials show strong segregation. At t=1 s, the mixture leaving the hopper consists mainly of pellets and nut coke. Shortly afterwards, the ratio of pellets and nut coke decreases, while sinter and subsequently lump ore become over-represented in the outlet mixture.

This behaviour can be explained by vertical segregation within the hopper. As shown in Fig. 15, the NMRs indicate that the bottom layer is predominantly composed of pellets and nut coke. At the beginning of discharge, these materials are released first. With continued discharge, material from the middle section, which is richer in sinter and lump ore, reaches the outlet, resulting in the observed increase in their NMRs.

The discharge pattern can be further explained by the hopper's core flow. Fig. 16 presents the particle velocity field, showing that particles in the central region move downwards while those near the hopper walls remain nearly stationary. This core flow

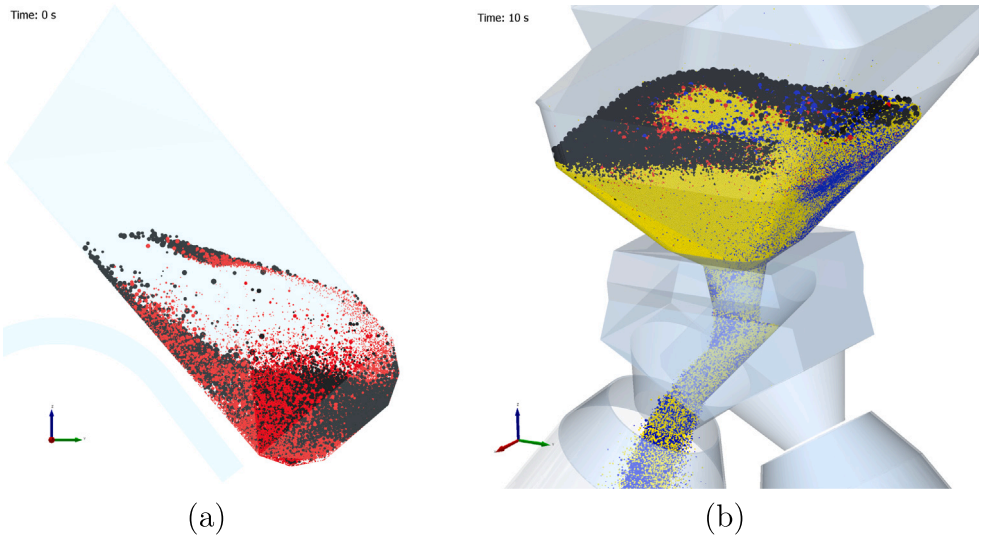

Fig. 12. (a) Spatial distribution of lump ore (red) and nut coke (black) within the skip car. Pellets and sinter are omitted for clarity. (b) Distribution of lump ore and nut coke at the surface of the burden within the receiving funnel.

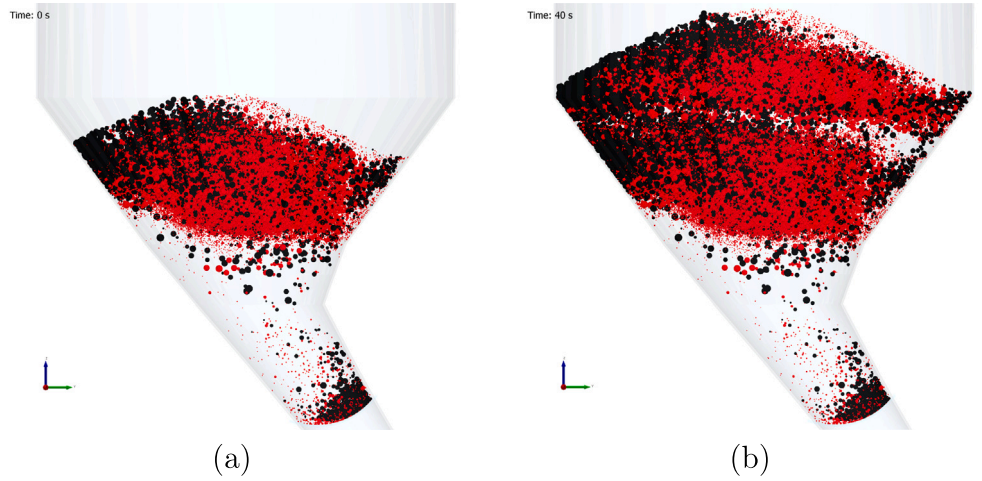

Fig. 13. Distribution of lump ore (red) and nut coke (black) within the top hopper after: (a) the first skip car load, and (b) the second skip car load. Pellets and sinter are omitted for clarity.

pattern is beneficial in this context, as the strong segregation present within the hopper is partly mitigated by the vertical mixing induced during the flow.

- **9–18 seconds:** At this stage, while pellets, sinter, and nut coke remain relatively well mixed, lump ore becomes over-represented due to the core flow within the hopper. As mentioned earlier, most lump ore particles are concentrated near the hopper's centre, whereas nut coke tends to move towards the hopper walls. Under core flow conditions, the lump ore concentrated in the centre is discharged first, making its NMR higher in the outlet flow.
- **18–30 seconds:** The most noticeable feature in this stage is the low mass ratio of sinter compared to the other materials. This occurs because, under core flow, the upper regions of the hopper, now reaching the outlet, contain a lower proportion of sinter (see Fig. 15(b)).
- **30–47 seconds:** Compared to the previous stage, the amount of sinter increases, while lump ore decreases at this stage. Pellets show a similar trend and remain relatively well mixed. The main observation in this stage is the under-representation of nut coke. This occurs because nut coke particles mostly accumulate near the hopper walls (see Fig. 13(b)), where particle motion is limited under core flow conditions. Consequently, these wall-adjacent particles remain in the hopper, while the centrally located material, characterised by a lower nut coke content, is discharged first, resulting in the observed under-representation of nut coke at the outlet.
- **47–53 seconds:** The sharp increase in the nut coke ratio at this stage is clearly observable. As noted earlier, this is because a large proportion of nut coke particles accumulate near the hopper walls (see Fig. 13(b)) and, under core flow conditions, are discharged last. An increase in the mass ratio of sinter is also noticed. To explain this, the distribution of pellets and sinter near the hopper walls should be examined. Fig. 17 shows the horizontal mass ratios of these materials within the hopper, indicating that

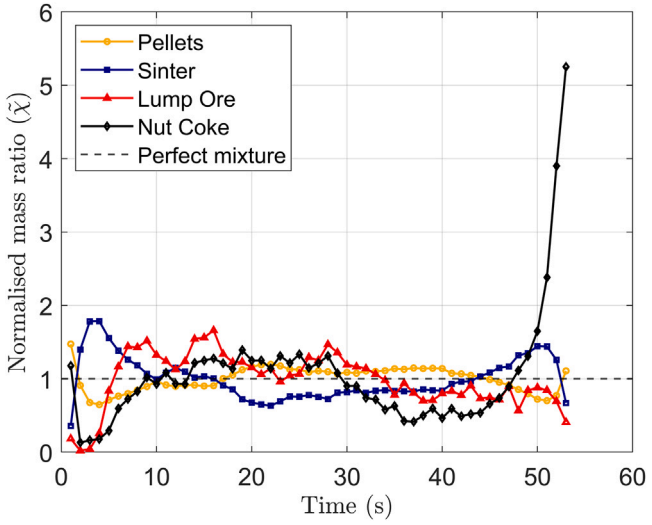

Fig. 14. NMR of different materials during top hopper discharging. The dashed line represents a perfect mixture.

the proportion of sinter near the walls is higher than that of pellets. This difference in the spatial distribution accounts for the observed increase in the sinter mass ratio during this stage.

In summary, the materials discharged from the top hopper show clear segregation, with the strongest segregation occurring during the initial and final stages. Among all materials, pellets display the least degree of segregation. It can be deducted that the observed segregation trends in Fig. 14 are closely related to the vertical segregation established within the hopper (see Fig. 15). During the intermediate stages, the core flow discharging pattern promotes partial mixing of lump ore and nut coke with pellets and sinter. Nevertheless, this core flow pattern causes the material located near the hopper walls to be discharged last, leading to pronounced segregation of nut coke and sinter towards the end of the discharge.

In the following subsections, each case listed in Table 1 is compared with the reference case to evaluate the effect of the varied factor in each case on segregation throughout the charging system.

3.3. Effect of hopper side (Case 2 vs. Case 1)

At Tata Steel IJmuiden, the ferrous materials are alternately discharged into the right and left hoppers. Up to this point, segregation has been evaluated for the left hopper. However, due to geometric asymmetry in the y-direction, associated with the configuration of the weighing bunkers and skip car (see Fig. 4), the segregation for the right hopper needs to be explored as well.

Fig. 18 presents the ΔRSD (see Eq. (6)) values for different materials, locations, and directions for the comparison of Case 2 to Case 1. As expected, since Case 2 deviates from Case 1 only after the receiving funnel, there is a negligible difference in the RSD value in the skip car.

Fig. 18 indicates that, overall, materials are more segregated in the right hopper compared to the left hopper, where segregation in the horizontal y-direction is particularly stronger. To examine this further, Fig. 19 presents the visual distribution of lump ore and nut coke particles in the left and right hoppers. Qualitatively, lump ore and nut coke appear to be more uniformly distributed in the left hopper; in the right hopper, the left area is noticeably thinned out in lump ore and nut coke.

For a quantitative assessment, the NMRs in the y-direction were compared with the reference case (Case 1) in Fig. 20. It confirms that pellets and sinter show stronger segregation in the right hopper. In particular, pellets are more concentrated on the left side of the right hopper, whereas in Case 1, they are well mixed in the corresponding region (right side in Case 1, due to mirroring).

To explain the pellet distribution, the average velocity of pellets in the y-direction was analysed immediately after leaving the receiving funnel, as they travel along the chute. This is the location where Case 2 deviates from Case 1. Fig. 21 presents a visual and quantitative comparison of the y-direction velocity of pellets for Cases 1 and 2, showing that the y-velocity in Case 2 is lower than in Case 1. This reduced y-velocity causes the pellets to be deposited more on the left side of the hopper, as also seen in Fig. 20(b).

The underlying mechanism can be related to the interaction between the pellet discharge direction and the chute orientation. When pellets are discharged from the skip car into the receiving funnel, they initially have velocity in the negative y-direction. In Case 1, the chute orientation aligns favourably with this velocity, facilitating smooth movement of pellets along the chute. In contrast, in Case 2, the chute orientation is unfavourable, which disrupts the flow. Consequently, this causes the accumulation of particles near the start of the chute, and reduces the flow velocity in the y direction.

When comparing segregation after the top hopper discharge between Case 1 and Case 2, Fig. 22 shows that the overall trends are generally similar. As discussed in Section 3.2, the segregation behaviour after hopper discharge is largely correlated to the vertical segregation established within the top hopper. This is supported by Fig. 18(c), which indicates only minimal differences in vertical segregation between the two cases. This similarity in the vertical distribution of materials explains the comparable segregation patterns observed in Fig. 22.

Despite these similarities, certain differences are observed. For most of the discharge period, pellets and sinter have lower segregation in Case 2. However, towards the end of discharge, both materials become more segregated. This can be attributed to differences in their horizontal mass ratio near the hopper walls between the two cases (Fig. 20). Since the material near the walls is discharged last, these horizontal differences directly influence the late-stage segregation behaviour.

Lump ore is also slightly more segregated in Case 2. For nut coke, as noted in Section 3.2, particles near the hopper walls are discharged last, causing a sharp increase in their proportion towards the end of discharge. This effect is even more pronounced in Case 2, where a greater quantity of nut coke is deposited near the walls compared to Case 1 (Fig. 19), which amplifies the late-stage rise in nut coke content.

In summary, although the system appears symmetric after the receiving funnel, the asymmetric charging geometry upstream (i.e., the weighing hoppers and skip car) changes the flow pattern and segregation behaviour. This results in increased segregation in the horizontal (y) direction within the top hopper. During hopper discharge, the overall segregation trends between the two cases are comparable; however, for Case 2, pellets and sinter are generally less segregated, whereas lump ore and nut coke show a slightly higher degree of segregation.

3.4. Effect of weighing bunker order (Case 3 vs. Case 1)

Discussions with experts at Tata Steel IJmuiden highlighted that the loading order of the weighing bunkers could be practically modified by discharging pellets into the sinter weighing bunker and, conversely, sinter into the pellets weighing bunker. It should be noted that this analysis concerns only pellets and sinter, as these materials are stored in separate weighing bunkers whose sequence can be altered in practice. Lump ore and nut coke are charged together into a smaller shared bunker that cannot accommodate the mass of pellets or sinter and were therefore not included in the order-variation analysis. Based on this insight, an alternative case was developed to evaluate whether this reversed loading order could reduce segregation in the skip car and, in turn, within the top hopper.

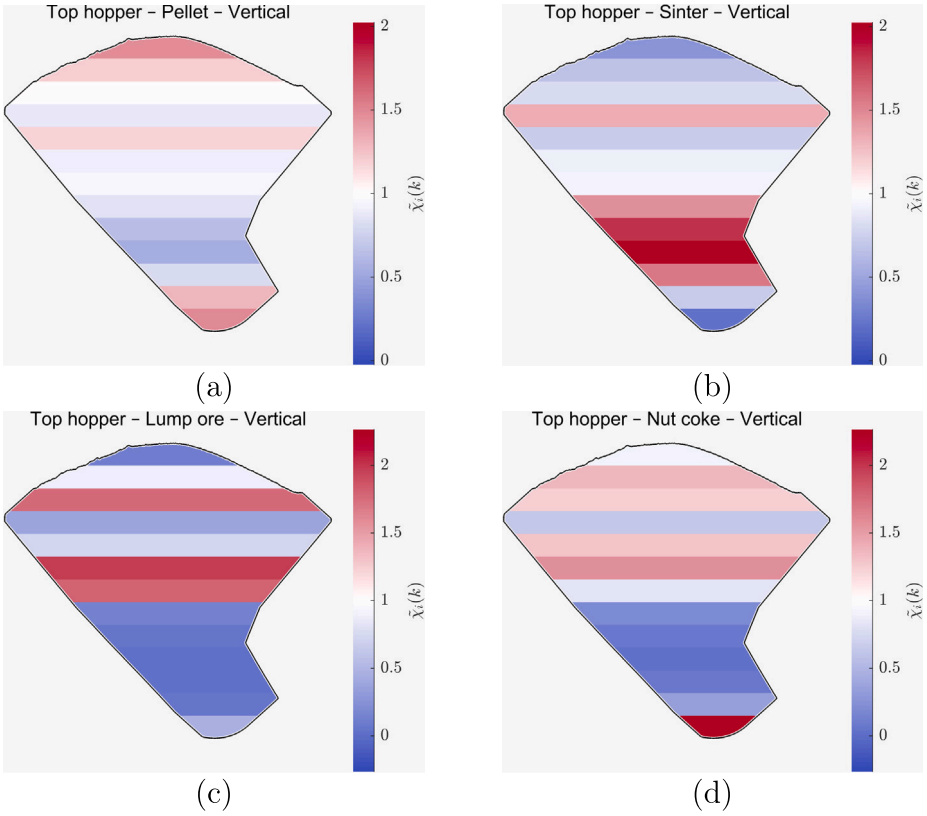

Fig. 15. NMR in the vertical direction of the top hopper for: (a) pellets, (b) sinter, (c) lump ore, and (d) nut coke.

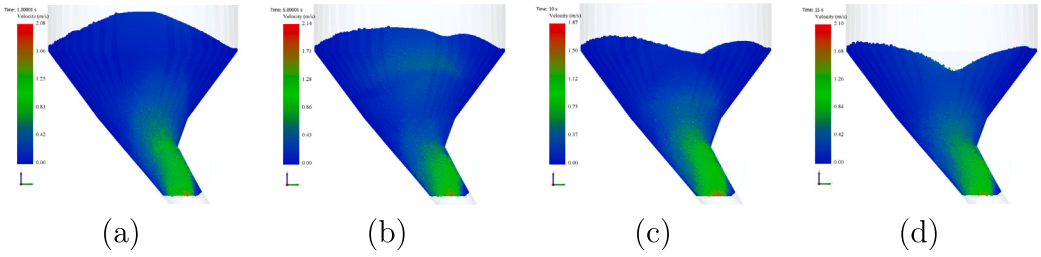

Fig. 16. Velocity field of the materials during hopper discharge at: (a) $t = 1$ s, (b) $t = 5$ s, (c) $t = 10$ s, and (d) $t = 15$ s. The same velocity scale (minimum and maximum values) is applied to all sub-figures to allow direct comparison.

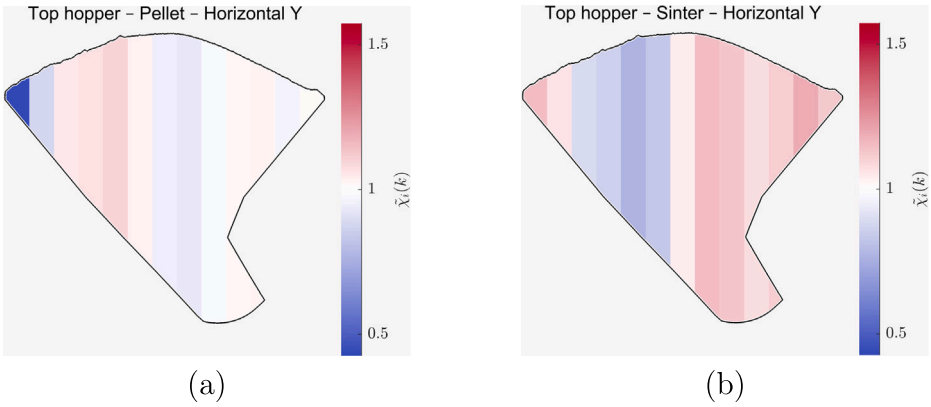

Fig. 17. NMRs in the y-direction within the top hopper for: (a) pellets, and (b) sinter.

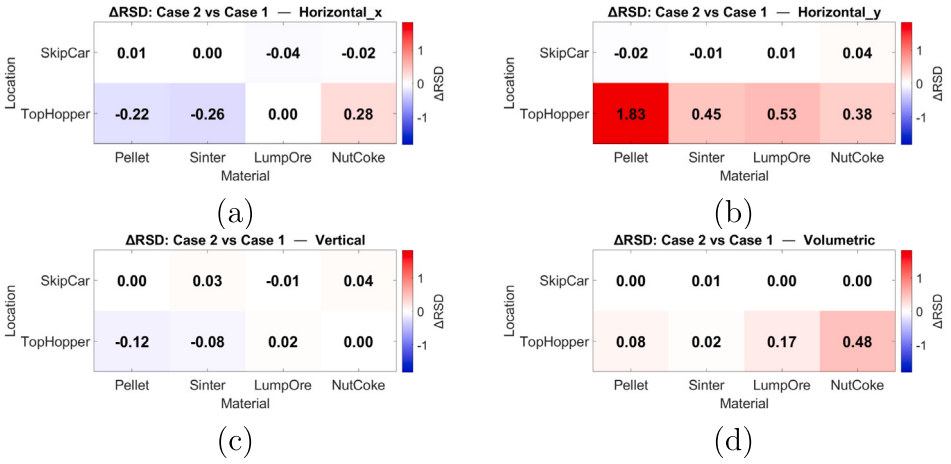

Fig. 18. Change in RSD for Case 2 vs. Case 1 in (a) Horizontal (X), (b) Horizontal (Y), (c) Vertical (Z), and (d) Volumetric directions.

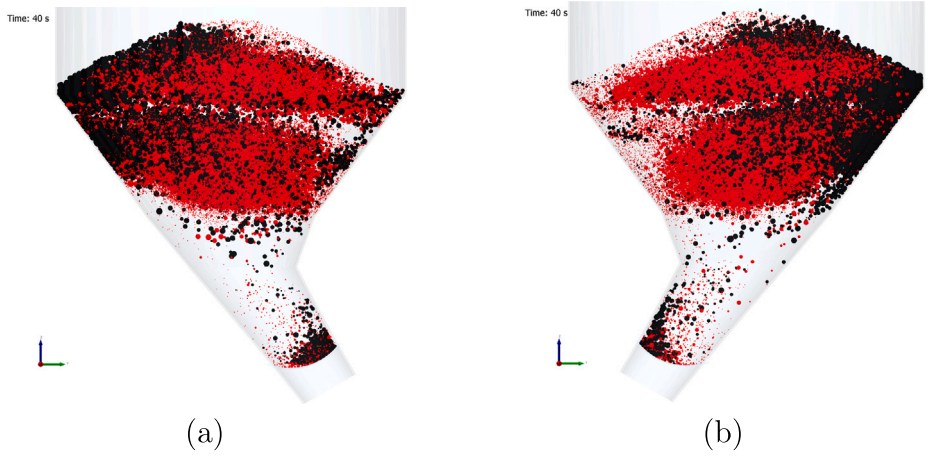

Fig. 19. Distribution of lump ore (red) and nut coke (black) within: (a) left, and (b) right top hoppers. Pellets and sinter are omitted for clarity.

Fig. 23 shows that reversing the weighing bunker order has varying effects depending on the material. For pellets, segregation increases within the skip car, while in the top hopper the increase is confined to the horizontal direction. For sinter, the impact on segregation is negligible. Lump ore also shows minimal change overall, although horizontal segregation in the x-direction is slightly higher. For nut coke, segregation within the skip car remains largely unchanged, while in the top hopper, horizontal segregation is slightly reduced.

Overall, these results show that reversing the order of the weighing bunkers is not advantageous, as it promotes mixing of pellets and sinter within the skip car and increases pellet segregation. However, nut coke shows less horizontal segregation, with a more uniform distribution in the top hopper, as illustrated in Fig. 24.

Fig. 25 shows that the segregation behaviour of the mixture discharged from the hopper differs significantly between Case 3 and Case 1 for pellets and sinter. As discussed earlier, segregation after hopper discharge is largely correlated with the vertical segregation established within the hopper. However, Fig. 23(c) shows that the extent of vertical segregation is not significantly altered in Case 3.

To provide a more complete understanding and gain deeper insight into the vertical distribution, the NMRs of pellets and sinter along the hopper height for Case 3 and Case 1 are presented in Fig. 26. It reveals that, although the vertical RSD values are similar, the distribution patterns differ substantially between the two cases. In Case 3, pellets are concentrated near the bottom of the hopper, while the upper region contains less pellets. This distribution explains the high NMR observed at the start of discharge, followed by a decline (see Fig. 25(a)). In contrast, for sinter, the bottom region has a lower mass ratio, resulting in reduced mass flow at the beginning. As discharge progresses and the top region—richer in sinter—is emptied, the mass ratio of sinter increases (Fig. 25(b)). This change in the discharge pattern could be either beneficial or detrimental, depending on the process requirements and the desired distribution of pellets and sinter on the furnace throat.

For lump ore and nut coke, however, both the trend and the extent of segregation are largely similar between the two cases. The only notable difference is observed for nut coke at the end of discharge, where segregation is reduced. This reduction is linked to the lower horizontal segregation of nut coke within the top hopper (see Fig. 24).

In summary, reversing the weighing bunkers of pellets and sinter increases segregation within the skip car, particularly for pellets. In the top hopper, it results in higher horizontal segregation of pellets but lower horizontal segregation of nut coke. After hopper discharge, the segregation behaviour of pellets and sinter is significantly affected, which is attributed to their significantly different vertical distributions in the hopper between the two cases. In contrast, lump ore and nut coke show overall similar segregation behaviour after hopper discharge in both cases.

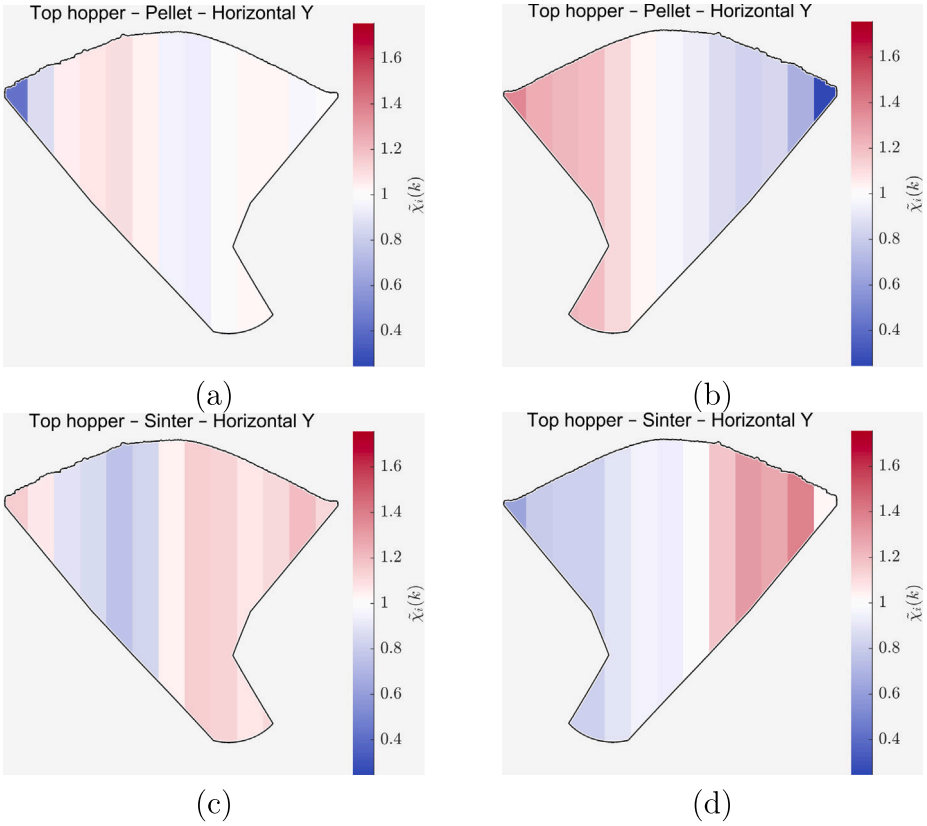

Fig. 20. NMR in the y-direction within the top hopper for: (a) pellets — left hopper, (b) pellets — right hopper, (c) sinter — left hopper, and (d) sinter — right hopper.

3.5. Effect of wall friction (Case 4 vs. Case 1)

At Tata Steel IJmuiden, parts of the internal surfaces of the charging equipment are lined with ceramic tiles to reduce wear, which are generally assumed to be smoother than steel. Although the joints or gaps between tiles may locally hinder flow, as is commonly observed in transfer chutes, the dominant effect is assumed to be a reduction in wall friction. It was shown in our previous study [47] that the particle–wall coefficient of sliding friction has a significant influence on segregation. To investigate this effect and assess whether the conclusions drawn from small-scale geometry can be translated to the full-scale system, Case 4 was defined and simulated with a 25% reduction in the particle–wall sliding friction coefficient for the tiled surfaces, and compared against the reference case (Case 1).

Fig. 27 shows that the reduction (by 25%) in the particle–wall sliding friction coefficient has an insignificant effect on segregation. The only noticeable change is a slight reduction in horizontal segregation in the x-direction within the top hopper. Similarly, Fig. 28 indicates that the segregation behaviour after hopper discharge remains largely unchanged. The main difference observed is a slightly faster discharge rate, due to the smoother internal surfaces in Case 4. These results suggest that, for the full-scale geometry considered, wall friction is not a dominant factor influencing segregation behaviour.

3.6. Effect of sinter PSD variability (Cases 5A and 6A vs. Case 1A)

At Tata Steel, the PSD of sinter varies over time. To investigate the effect of these variations on the segregation of the ferrous mixture, three simulation cases were defined and performed: Case 1A, representing the average yearly PSD (reference case); Case 5A, representing the finest monthly PSD; and Case 6A, representing the coarsest monthly PSD, taken as two extremes. The particle size distributions of these variants are illustrated in Fig. 29, and the exact PSD values are listed in Table A.5 in Appendix.

Figs. 30 and 31 show that variations in sinter PSD have no significant overall effect on the extent of segregation; nevertheless, minor differences can be observed. The finer PSD in Case 5A results in slightly higher segregation, which can be attributed to enhanced percolation and reduced interlocking of smaller particles. In contrast, the coarser PSD in Case 6A leads to slightly lower segregation, particularly in the y-direction within the top hopper, as the larger particles exhibit greater stability and reduced tendency to percolate.

To explain the differences in y-direction segregation of sinter within the top hopper, Fig. 32 presents the horizontal distribution of sinter for the three cases. For the finer PSD (Case 5A), more sinter accumulates on the right side of the hopper and less on the left. The opposite trend is observed in Case 6A with the coarser PSD. Since the extent of segregation within the skip car is largely the same across all cases (Figs. 30 and 31), these horizontal differences in the top hopper are most likely induced by the chute flow. Larger particles are able to maintain higher momentum and therefore travel farther after leaving the chute. As a result, in Case 6A with the coarser PSD, more sinter particles are deposited on the left side of the hopper than in Cases 5A and 1A, as shown in Fig. 32. This suggests that chute dynamics can amplify relatively small differences in PSD into noticeable variations in horizontal distribution within the hopper.

Fig. 33 illustrates the segregation of different materials after hopper discharge. The overall segregation behaviour is largely similar across the cases, with the main differences appearing in the final stage of discharge, particularly for pellets and sinter. For sinter, it is observed

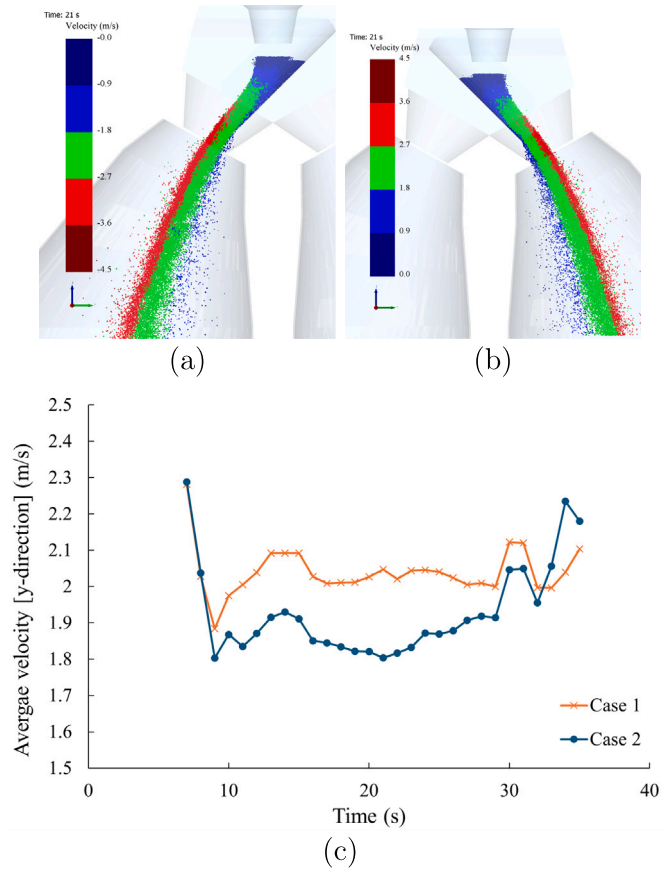

Fig. 21. Visualisation of the velocity of pellets in the horizontal y-direction on the chute for a single time instance in (a) Case 1 and (b) Case 2. (c) Average velocity of pellets in the y-direction on the chute over the entire flow period.

that the finer the PSD, the lower the segregation towards the end of the discharge. This can be explained by the horizontal segregation in the y-direction within the top hopper, as discussed above. As shown in Fig. 32(c), in the case of the coarser PSD (Case 6A), more sinter is deposited on the left side of the hopper. As concluded in Section 3.2, the material located near the hopper walls is discharged last, which leads to an increase in the sinter content at the outlet in Case 6A. This indicates that finer PSDs may help mitigate late-stage segregation, whereas coarser PSDs tend to exacerbate it.

In summary, variations in the PSD of sinter primarily affect the horizontal distribution of material within the top hopper. A coarser PSD results in particles travelling farther from the chute and accumulating on the left side of the hopper. This, in turn, increases segregation during the final stage of hopper discharge. Nevertheless, PSD variation of sinter had only a minor overall influence on segregation behaviour in the charging system.

3.7. Effect of lump ore type (Case 7 vs. Case 1)

At Tata Steel IJmuiden, several types of lump ore (designated as A–E) are used. In typical operations, types A–C are most common, where types A and B have similar particle size distributions (PSDs), and type C is slightly finer (see Table A.3). To assess whether this difference affects segregation within the charging system, Case 7 was modelled using lump ore type C.

Fig. 34 shows that changing the lump ore type has a negligible effect on segregation behaviour in both the skip car and the top hopper. Minor variations fall within the expected range of simulation variability. Moreover, segregation after hopper discharge shows negligible differences relative to Case 1 (see Appendix, Fig. A.39).

In this comparison, the only parameter varied between the two ore types was the particle size distribution (PSD). If variations in other properties, such as particle density and friction coefficients, were also considered, the effect might have been more pronounced. Nevertheless, under the current operating conditions, the lump ore type is not a significant factor influencing segregation

3.8. Effect of sinter particle shape (Case 8 vs. Case 1)

So far, spherical particles have been used to represent all materials because of their computational efficiency, which is essential for simulating large-scale systems. This simplification is broadly effective, particularly for pellets that are nearly spherical. However, other ferrous materials such as sinter, lump ore, and nut coke exhibit irregular shapes (see Fig. 1). To evaluate whether accounting for particle shape influences segregation behaviour, sinter, which is the largest fraction among these materials, was selected for more detailed representation. This was achieved using a clumped-sphere approach (see Fig. 3). This particle shape was adopted because it had been successfully calibrated and validated for sinter particles in our previous study [44], where the selected number of sub-spheres was shown to provide a good balance between realistic shape representation and computational efficiency.

Fig. 35 shows that the irregular shape of sinter mainly affects the segregation of pellets and sinter, while lump ore and nut coke remain largely unchanged. This is because their total amount is much smaller than that of pellets and sinter, which limits their interaction with sinter particles during discharge from the weighing bunkers into the skip car. In the skip car, vertical segregation of pellets and sinter is slightly higher in Case 8. A more detailed view is provided in Fig. 36, which illustrates that non-spherical sinter particles in Case 8 are distributed more extensively near the surface of the skip car. This happens because the non-spherical sinter particles discharge more slowly from the weighing bunker, resulting in a larger proportion of sinter being deposited towards the end of the filling process of the skip car. Consequently, a greater amount of sinter accumulates in the upper region of the skip car. Although this increases the vertical RSD in the skip car in Case 8, it reduces vertical segregation within the top hopper. As shown in Fig. 37, the bottommost part of the top hopper, which is relatively depleted of sinter in Case 1, is now populated with more sinter in Case 8, leading to a more balanced vertical distribution.

Fig. 38 highlights the effects of modelling sinter as nonspherical particles. First, the hopper discharge time is prolonged, reflecting a slower flow regime induced by the enhanced interlocking and higher effective resistance of irregularly shaped particles. Second, the segregation behaviour during the mid-discharge period remains largely consistent with Case 1. The main differences are observed during the initial stage of discharge, where the NMR of pellets at the outlet decreases significantly, while that of sinter increases. This observation is explained by the vertical composition at the bottom of the hopper (see Fig. 37), where in Case 8 a greater proportion of sinter and fewer pellets are present. Beyond this initial stage, the influence of particle shape diminishes, with only minor and inconsistent differences observed thereafter.

In summary, modelling sinter particles as non-spherical shapes affected only the segregation behaviour of pellets and sinter, as lump ore and nut coke are present in much smaller quantities and thus have limited interaction with sinter. The main effect is on the vertical segregation within the skip car and top hopper, which subsequently affects segregation after hopper discharge only during the initial stage. Beyond this, overall segregation trends remain comparable to the spherical-particle case. These findings suggest that while accounting for particle shape improves realism and is relevant for capturing early-stage discharge dynamics, spherical particles remain adequately accurate for representing large-scale segregation behaviour in the charging system.

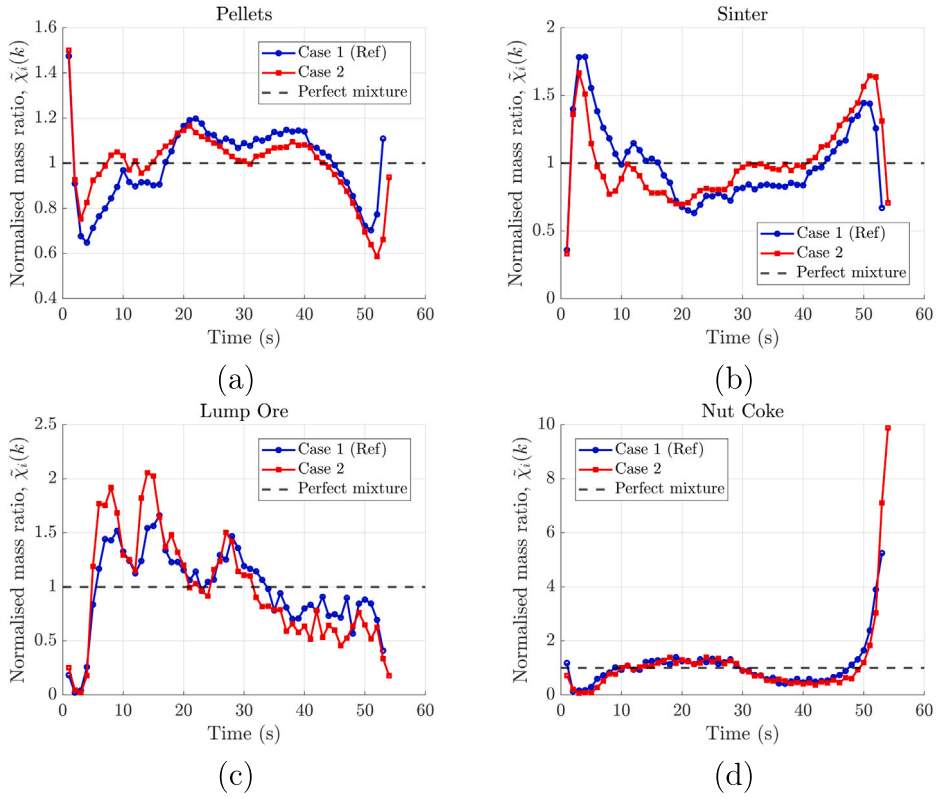

Fig. 22. Comparison of segregation after hopper discharge between Case 2 and the reference case (Case 1) for: (a) pellets, (b) sinter, (c) lump ore, and (d) nut coke.

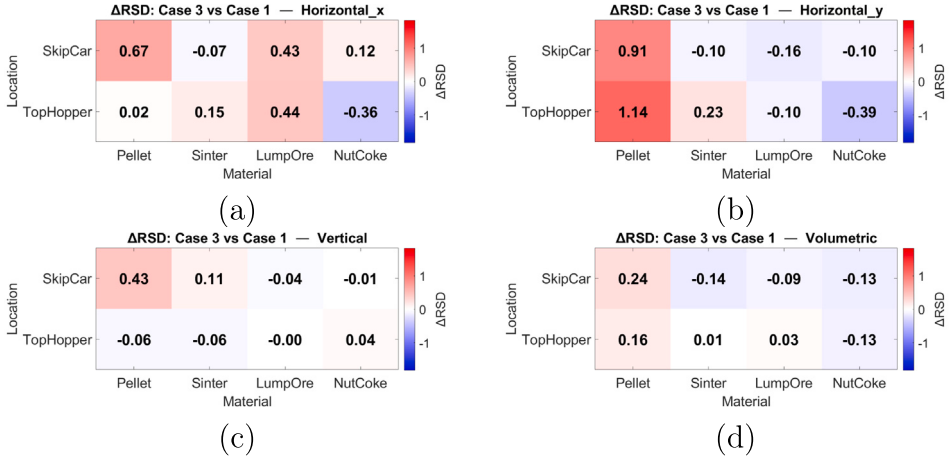

Fig. 23. Change in RSD for Case 3 vs. Case 1 in (a) Horizontal (X), (b) Horizontal (Y), (c) Vertical (Z), and (d) Volumetric directions.

4. Conclusion

This study presented the results of industrial-scale DEM simulations of segregation in the ferrous mixture (pellets, sinter, lump ore, and nut coke) within the blast furnace charging system, from the weighing bunkers through to discharge from the top hopper. A reference case, reflecting the current practice at Tata Steel IJmuiden, was first modelled and analysed in detail to establish the baseline segregation behaviour. Building on this, a series of systematically designed case studies was carried out to investigate the influence of various factors, including material properties, modelling assumptions, and operational parameters, on segregation. The conclusions of this study are summarised below:

- Segregation generally decreases from the skip car to the top hopper, due to partial remixing occurring during transfer through the receiving funnel.
- Pellets and sinter exhibit lower segregation levels than lump ore and nut coke, with sinter slightly more segregated than pellets.

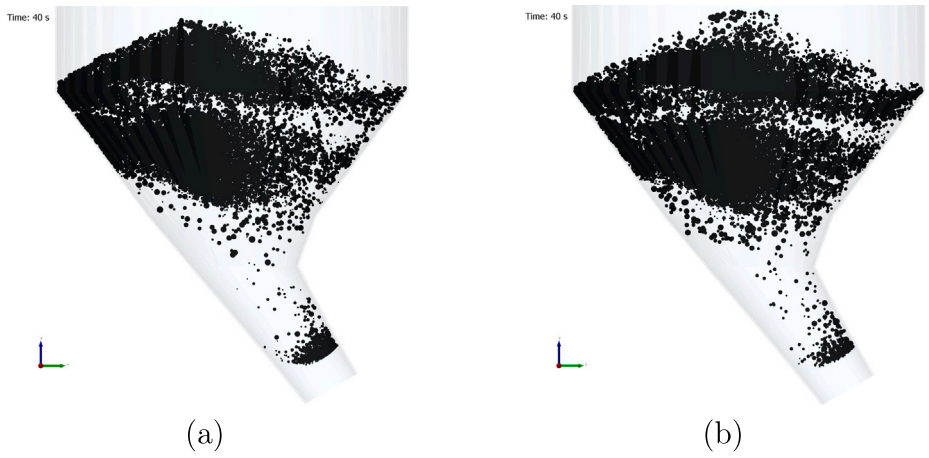

Fig. 24. Distribution of nut coke within the top hopper for: (a) Case 1, and (b) Case 3.

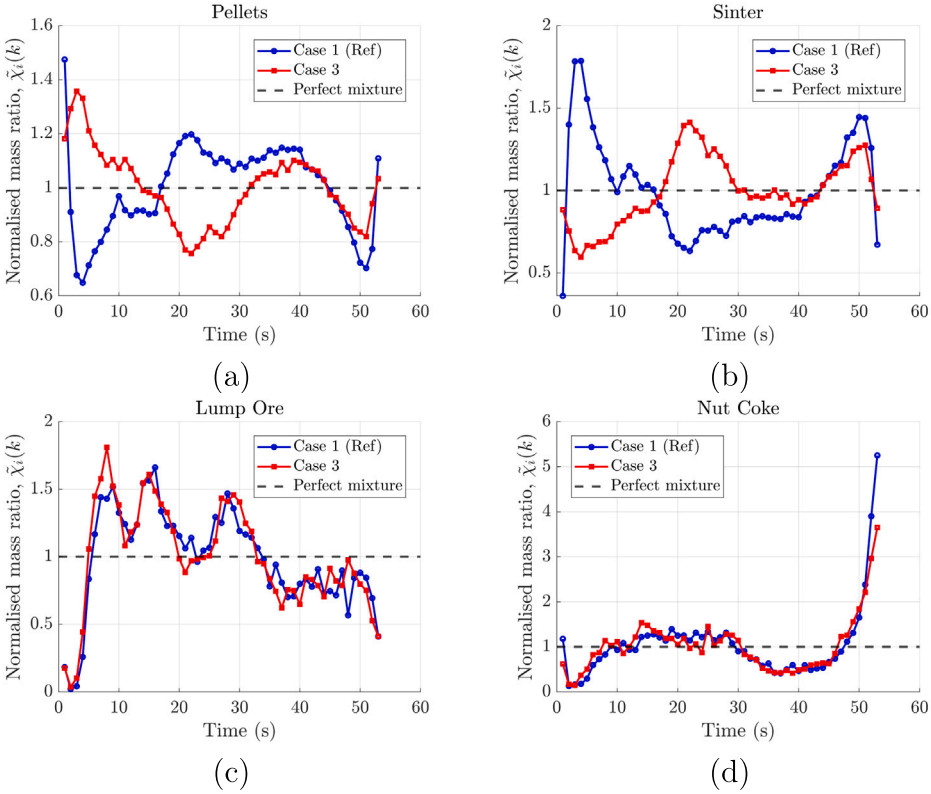

Fig. 25. Comparison of segregation after hopper discharge between Case 3 and the reference case (Case 1) for: (a) pellets, (b) sinter, (c) lump ore, and (d) nut coke.

Specifically, lump ore and nut coke show strong vertical segregation within the top hopper, where they mostly accumulate near the top surface of the mixture.

- Significant segregation was observed during top hopper discharge, particularly at the beginning and end stages. Among all materials, pellets consistently showed the lowest degree of segregation. The results also indicated that segregation behaviour during discharge was largely correlated to the vertical distribution of the mixture within the hopper.
- The mixture charged into the right hopper showed stronger horizontal (y) segregation than that charged into the left hopper, because of geometric asymmetry and the mirrored orientation of the chute. During hopper discharge, however, the overall segregation patterns remain similar in both cases. The main difference is

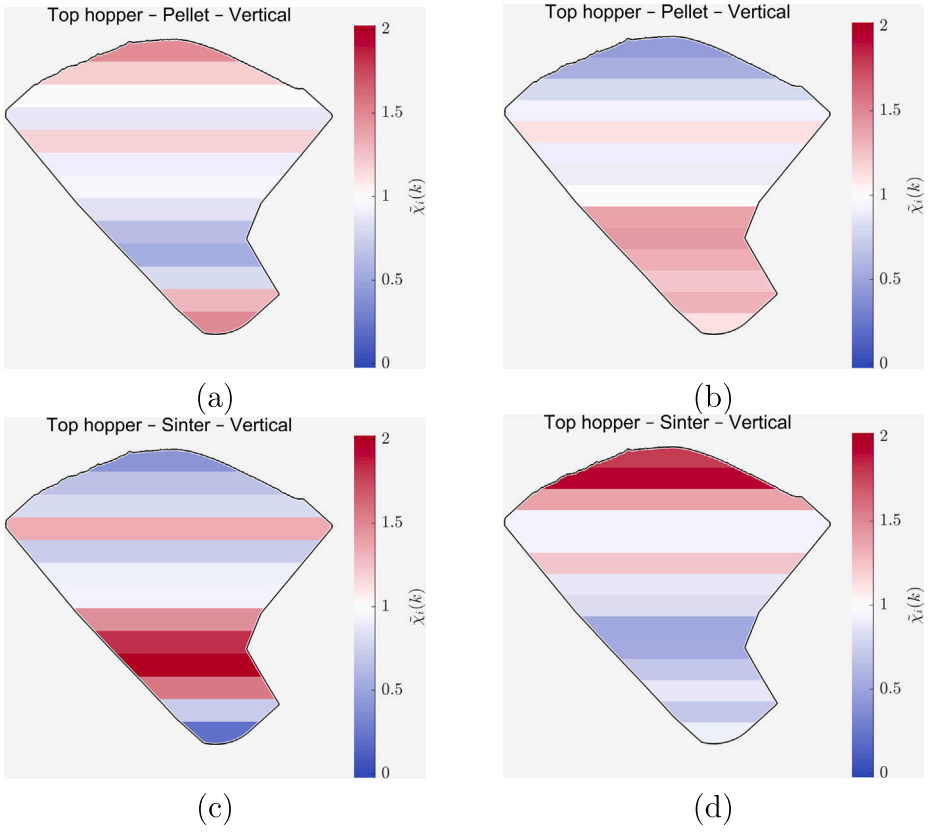

Fig. 26. NMR in the vertical direction within the top hopper for: (a) pellets — Case 1, (b) pellets — Case 3, (c) sinter — Case 1, and (d) sinter — Case 3.

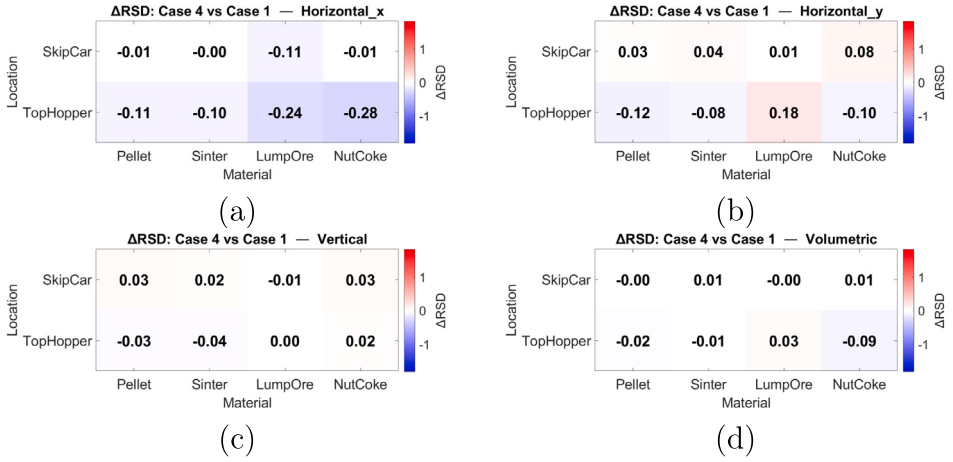

Fig. 27. Change in RSD for Case 4 vs. Case 1 in (a) Horizontal (X), (b) Horizontal (Y), (c) Vertical (Z), and (d) Volumetric directions.

that pellets and sinter become slightly less segregated, while lump ore and nut coke show a slightly higher degree of segregation.

- Reversing the order of pellets and sinter in the weighing bunkers increases segregation in the skip car, particularly for pellets. In the top hopper, it leads to greater horizontal segregation of pellets while slightly reducing the segregation of nut coke. Moreover, it changes the vertical distribution of pellets and sinter, which in turn significantly influences their segregation behaviour during hopper discharge. By contrast, lump ore and nut coke show segregation patterns that are largely consistent with those of the reference case.
- Varying the PSD of sinter had only a minor effect on segregation in the skip car and top hopper. Finer PSDs (i.e., with smaller D_{50}) led to slightly higher segregation, while coarser PSDs gave slightly lower segregation, particularly in the y-direction within the top

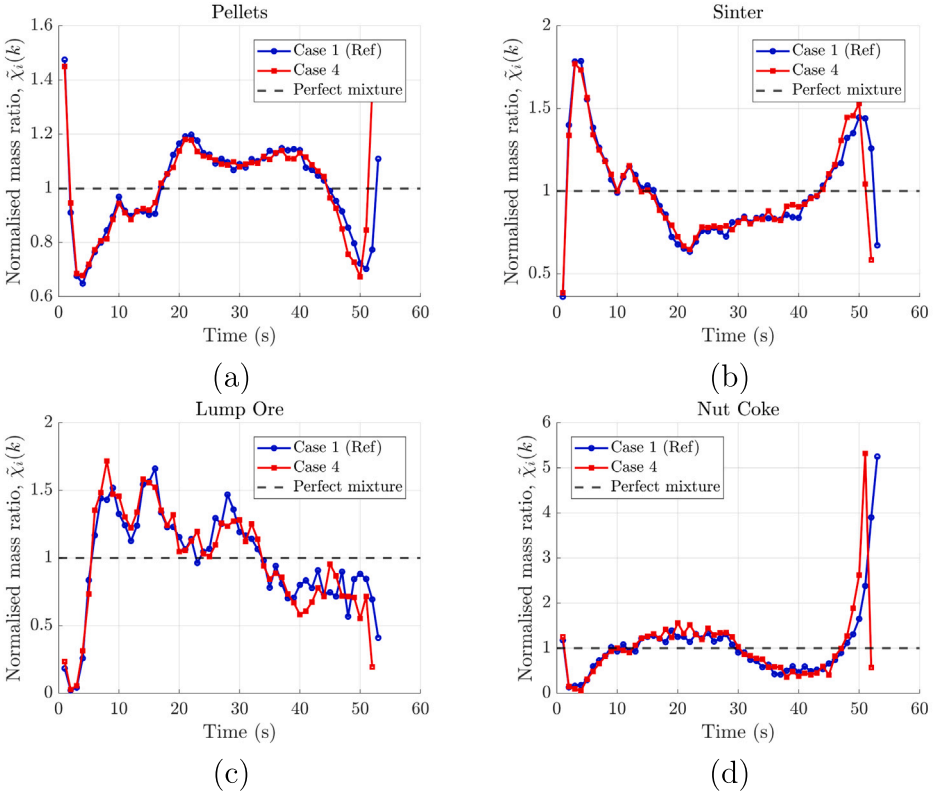

Fig. 28. Comparison of segregation after hopper discharge between Case 4 and the reference case (Case 1) for: (a) pellets, (b) sinter, (c) lump ore, and (d) nut coke.

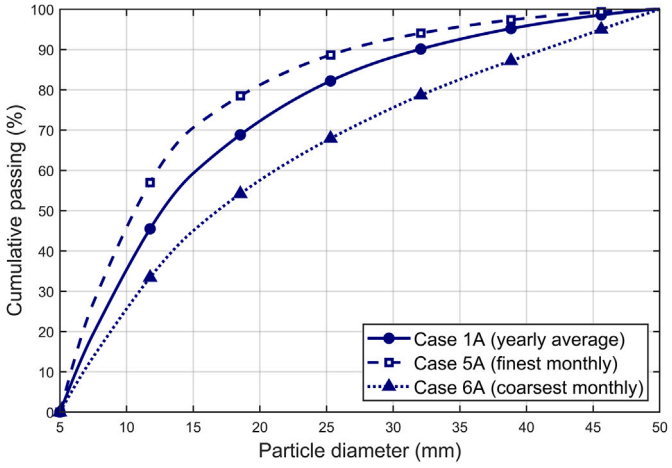

Fig. 29. Particle size distributions of sinter used in Cases 1A (yearly average), 5A (finest monthly), and 6A (coarsest monthly).

hopper. During hopper discharge, differences appeared only in the final stage, where the finer PSD (smaller D_{50}) produced less segregation than the coarser PSD.

- Modelling sinter as non-spherical (clumped) particles mainly affected the segregation of pellets and sinter. It altered their vertical distribution in the top hopper, which in turn influenced the initial stage of hopper discharge, where more sinter and fewer pellets were discharged compared to the spherical case. The discharge time also increased, as expected, due to particle interlocking and slower flow velocity. Beyond the initial stage, however, the effect of non-spherical sinter on segregation was negligible, indicating that spherical particles were sufficiently accurate for representing large-scale behaviour.
- Reducing wall friction and changing the lump ore type both had negligible effects on segregation. The only noticeable change was a slightly faster discharge when wall friction was reduced.

Overall, these findings provide new insights into the factors influencing multi-component segregation in industrial blast furnace charging. They demonstrate that while some factors (e.g., weighing bunker order) can substantially influence segregation patterns, others (e.g., wall friction, lump ore type, or moderate PSD variations) play only a minor role. Importantly, the results highlight the central role of upstream conditions in determining downstream segregation behaviour: promoting homogeneity in the weighing bunkers or early charging stages offers the greatest potential for mitigating segregation throughout the system. These outcomes not only advance the fundamental understanding of segregation in large-scale multi-component flows but also provide a foundation for developing practical strategies to mitigate segregation in industrial practice. Nevertheless, further work is required to validate the model comprehensively against high-quality data from BF charging systems, in order to ensure accurate and reliable numerical predictions, and to extend the present study towards analysing burden distribution at the blast furnace throat, which is a critical region for assessing overall charging performance.

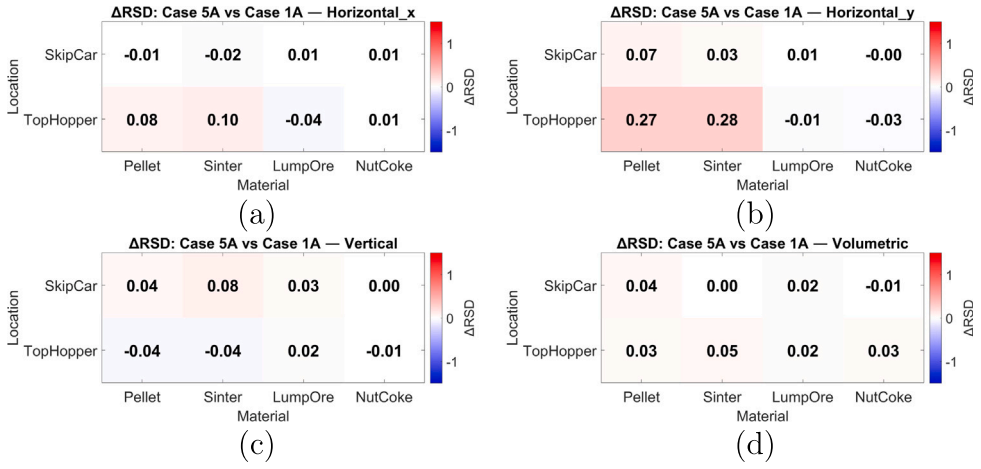

Fig. 30. Change in RSD for Case 5A vs. Case 1A in (a) Horizontal (X), (b) Horizontal (Y), (c) Vertical (Z), and (d) Volumetric directions.

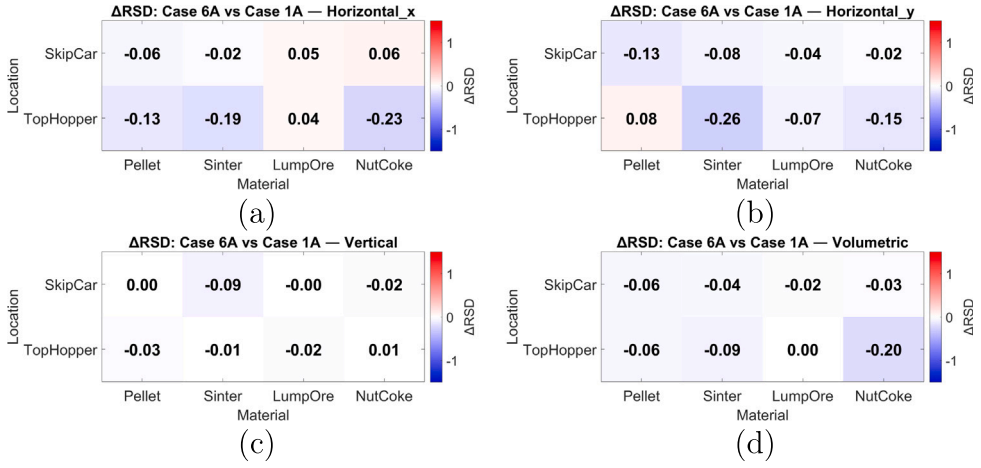

Fig. 31. Change in RSD for Case 6A vs. Case 1A in (a) Horizontal (X), (b) Horizontal (Y), (c) Vertical (Z), and (d) Volumetric directions.

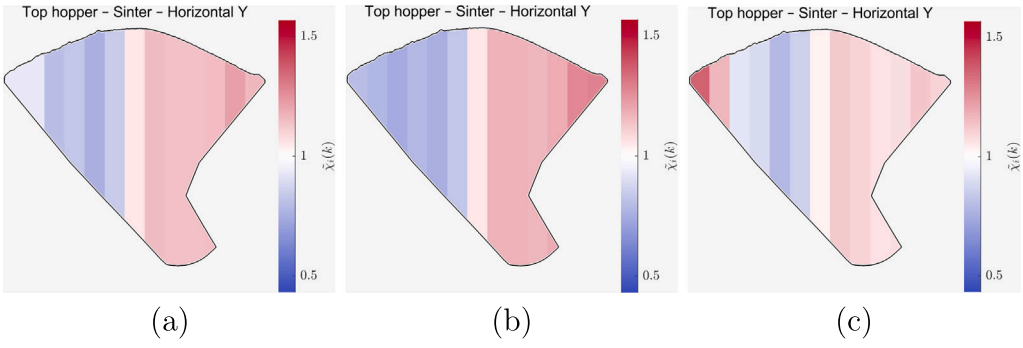

Fig. 32. NMR in the horizontal y direction within the top hopper for: (a) Case 1A (average PSD), (b) Case 5A (fine PSD), and (c) Case 6A (coarse PSD).

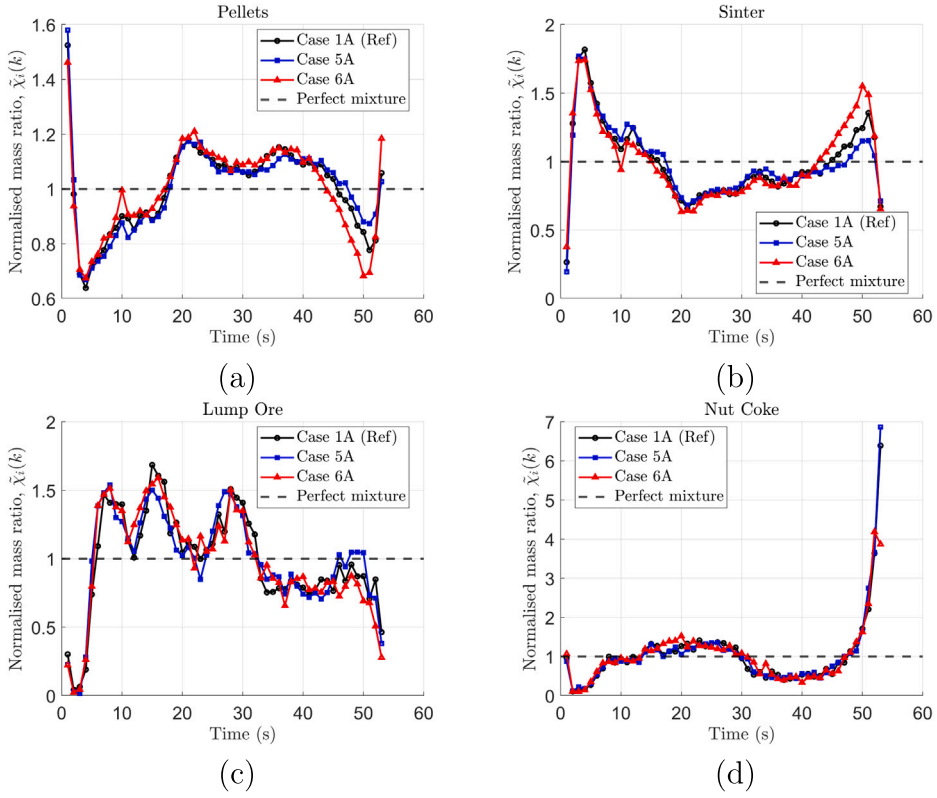

Fig. 33. Comparison of segregation after hopper discharge between Case 5A, Case 6A, and their reference case (Case 1A) for: (a) pellets, (b) sinter, (c) lump ore, and (d) nut coke.

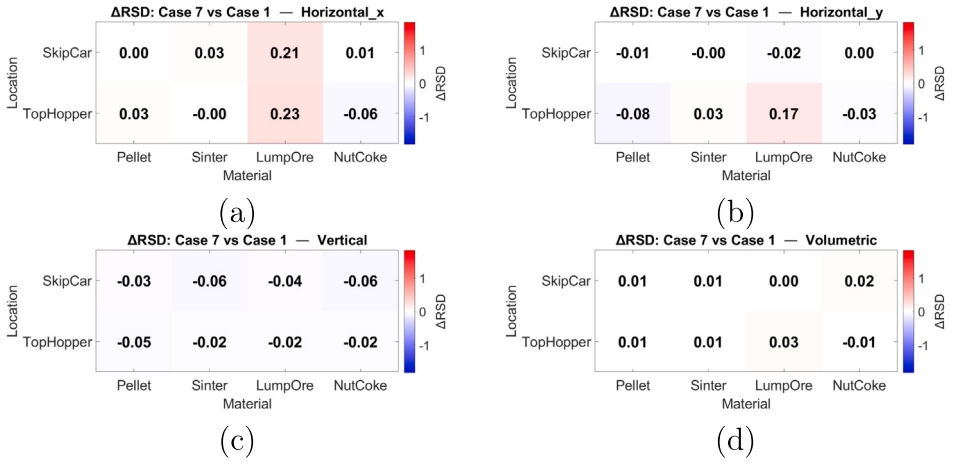

Fig. 34. Change in RSD for Case 7 vs. Case 1 in (a) Horizontal (X), (b) Horizontal (Y), (c) Vertical (Z), and (d) Volumetric directions.

CRediT authorship contribution statement

Ahmed Hadi: Writing – review & editing, Writing – original draft, Visualization, Validation, Software, Methodology, Investigation, Formal analysis, Data curation, Conceptualization. **Yusong Pang:** Writing – review & editing, Supervision. **Allert Adema:** Validation, Formal analysis, Data curation, Conceptualization. **Jan van der Stel:** Validation, Formal analysis, Data curation, Conceptualization. **Dingena Schott:** Writing – review & editing, Visualization, Supervision, Resources, Project administration, Methodology, Investigation, Funding acquisition, Formal analysis, Conceptualization.

Declaration of competing interest

The authors declare that they have no known competing financial interests or personal relationships that could have appeared to influence the work reported in this paper.

Acknowledgements

This research was carried out under project number T18019 in the framework of the Research Program of the Materials innovation institute (M2i) (www.m2i.nl) supported by the Dutch government.

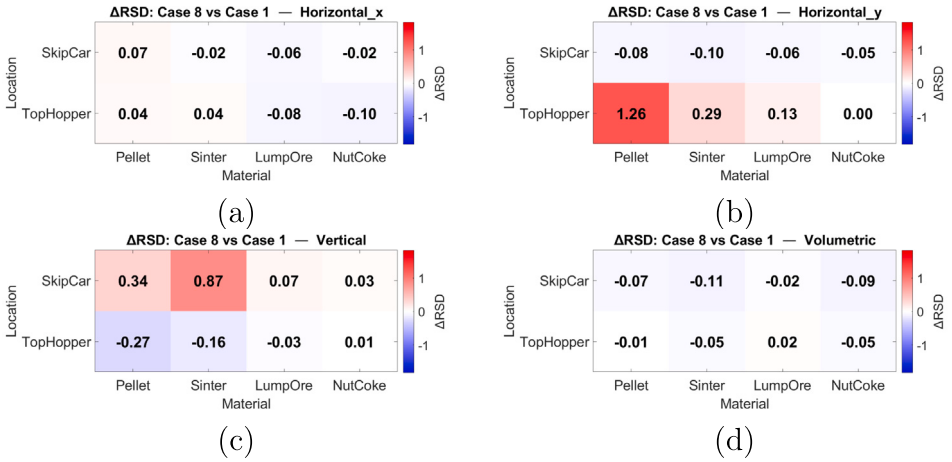

Fig. 35. Change in RSD for Case 8 vs. Case 1 in (a) Horizontal (X), (b) Horizontal (Y), (c) Vertical (Z), and (d) Volumetric directions.

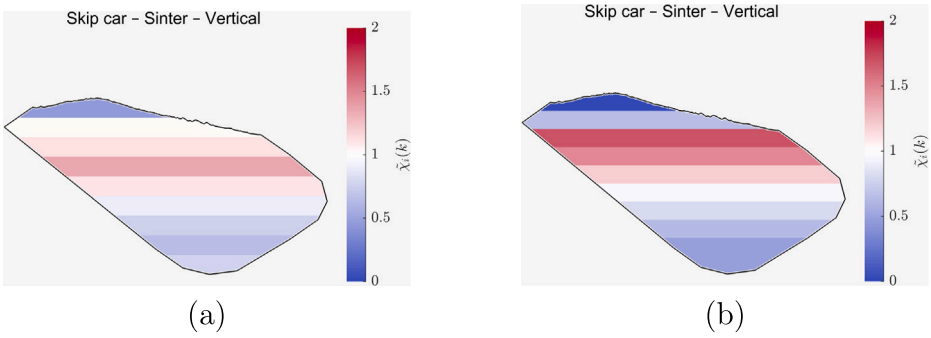

Fig. 36. NMR of sinter in the vertical direction within the skip car for: (a) Case 1, and (b) Case 8.

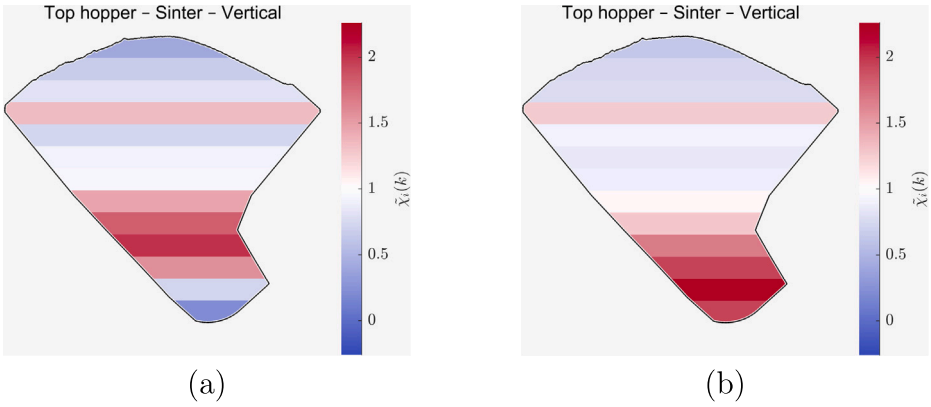

Fig. 37. NMR in the vertical direction within the top hopper for: (a) Case 1, and (b) Case 8.

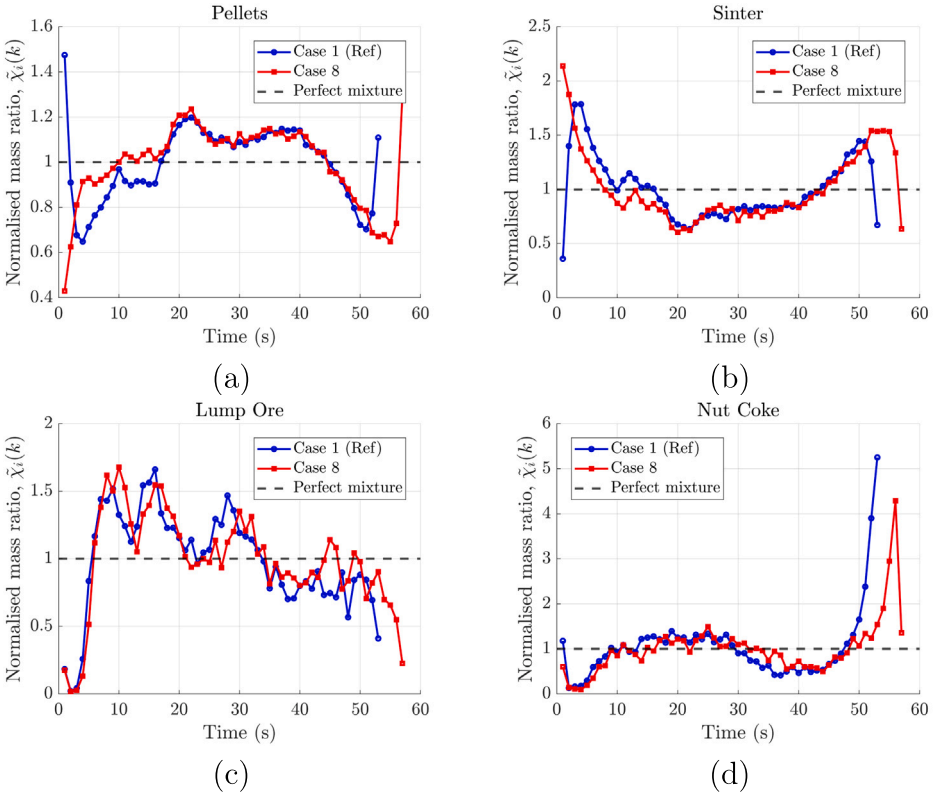

Fig. 38. Comparison of segregation after hopper discharge between Case 8 and the reference case (Case 1) for: (a) pellets, (b) sinter, (c) lump ore, and (d) nut coke.

Table A.3
Particle-size distributions (PSD, mass %) of all materials.

Pellets		Sinter		Lump ore (A,B)		Lump ore (C)		Nut coke	
Size (mm)	%	Size (mm)	%	Size (mm)	%	Size (mm)	%	Size (mm)	%
6.35–9.5	10	5–10	30	5–8	4.56	5–8	3.71	10–16	5
9.5–11.2	40	10–20	40	8–10	4.88	8–10	3.67	16–30	45
11.2–12.5	40	20–40	20	10–16	16.46	10–16	23.88	30–45	45
12.5–15	10	40–50	10	16–20	11.58	16–20	16.85	45–50	5
–	–	–	–	20–25	16.14	20–25	20.56	–	–
–	–	–	–	25–31.5	21.32	25–31.5	21.71	–	–
–	–	–	–	31.5–40	19.09	31.5–40	8.88	–	–
–	–	–	–	40–50	5.97	40–50	0.74	–	–

Table A.4
DEM parameters used in the simulations.

Parameter		Pellets	Sinter	Lump ore	Nut coke	Geometry
Solid density (kg/m^3)		3350	3208	4231	1118	7800
Young's modulus (Pa)		1.0×10^8	1.0×10^8	1.0×10^8	1.0×10^8	1.0×10^{11}
Poisson's ratio		0.25	0.25	0.21	0.22	0.30
Static friction coefficient [μ_s]						
	Pellets	0.73	0.815	0.665	0.80	0.90
	Sinter	–	0.90	0.75	0.885	0.83
	Lump ore	–	–	0.60	0.735	0.69
	Nut coke	–	–	–	0.87	0.41
Rolling friction coefficient [μ_r]						
	Pellets	0.12	0.16	0.095	0.135	0.16
	Sinter	–	0.20	0.135	0.175	0.20
	Lump ore	–	–	0.07	0.11	0.09
	Nut coke	–	–	–	0.15	0.09

(*continued on next page*)

Table A.4 (*continued*).

Parameter		Pellets	Sinter	Lump ore	Nut coke	Geometry
Restitution coefficient [C_r]						
	Pellets	0.76	0.555	0.585	0.555	0.70
	Sinter	–	0.35	0.38	0.35	0.40
	Lump ore	–	–	0.41	0.38	0.43
	Nut coke	–	–	–	0.35	0.20
Time step (s)	2.909×10^{-5} (30% of Rayleigh time step)					

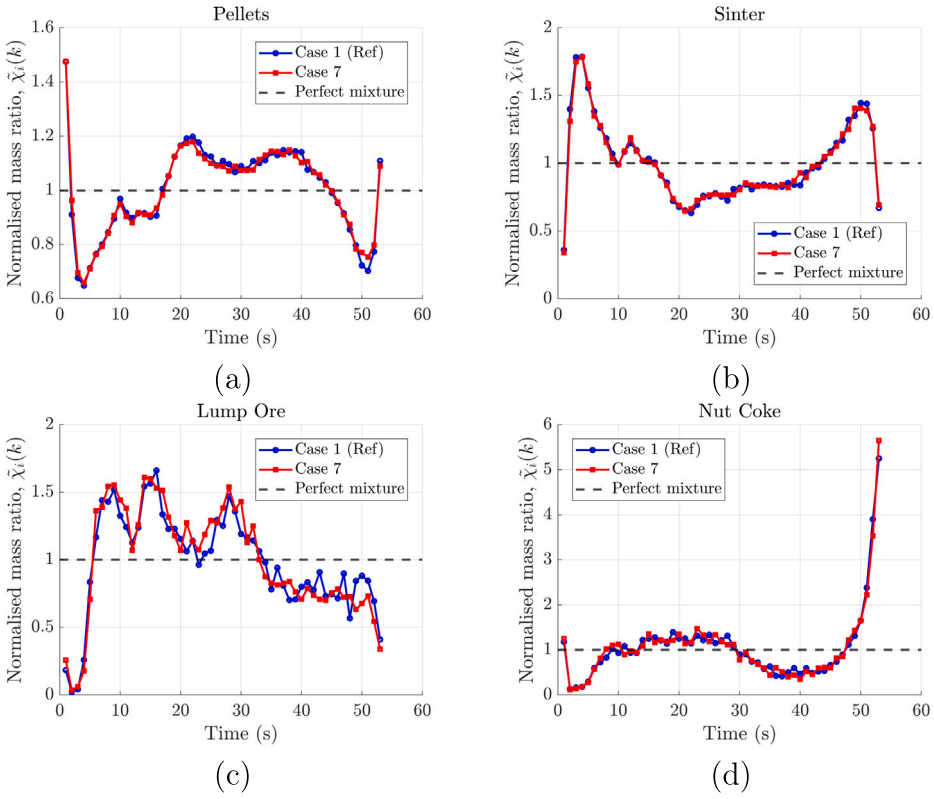

Fig. A.39. Comparison of segregation after hopper discharge between Case 7 and the reference case (Case 1) for: (a) pellets, (b) sinter, (c) lump ore, and (d) nut coke.

Table A.5
Different PSDs of sinter used in Cases 1A, 5A, and 6A.

Size (mm)	Sinter (updated)	Sinter (fine)	Sinter (coarse)
5–10	38.9	54.1	27.4
10–20	40.7	33.0	35.2
20–40	17.1	11.3	26.0
40–50	3.3	1.6	11.4

Appendix

See Tables A.3–A.5 and Fig. A.39.

Data availability

Data will be made available on request.

References

[1] Y. Yu, H. Saxén, Experimental and DEM study of segregation of ternary size particles in a blast furnace top bunker model, Chem. Eng. Sci. 65 (2010) 5237–5250, http://dx.doi.org/10.1016/j.ces.2010.06.025.

[2] T. Bhattacharya, J.J. McCarthy, Chute flow as a means of segregation characterization, Powder Technol. 256 (2014) 126–139, http://dx.doi.org/10.1016/j.powtec.2014.01.092.

[3] A. Spence, Improving Blast Furnace Burden Distribution by Stockfeed Segregation Control (Ph.D. thesis), University of Wollongong, 1996.

[4] H. Mio, Y. Narita, K. Nakano, S. Nomura, Validation of the burden distribution of the 1/3-scale of a blast furnace simulated by the discrete element method, Processes 8 (2020) 6, http://dx.doi.org/10.3390/pr8010006.

[5] Y. Kajiwara, T. Jimbo, T. Joko, Y.-i. AMINAGA, T. Inada, Investigation of bell-less charging based on full scale model experiments, Trans. Iron Steel Inst. Jpn. 24 (10) (1984) 799–807.

[6] W. Xu, S. Cheng, C. Li, Experimental study of the segregation of burden distribution during the charging process of bell-less top blast furnace with two parallel hoppers, in: Journal of Physics: Conference Series, vol. 2044, IOP Publishing, 2021, 012129.

[7] J. Chen, H. Zuo, Q. Xue, J. Wang, A review of burden distribution models of blast furnace, Powder Technol. 398 (2022) http://dx.doi.org/10.1016/j.powtec.2021.117055.

[8] X. Zhang, N. Wang, Z. Zhou, Z. Ning, M. Chen, Effect of combined ferrous burden composition and ore-coke interaction on blast furnace burden distribution, Powder Technol. 449 (2025) 120416.

[9] C.X. Li, K.J. Dong, S.D. Liu, G.R. Chandratilleke, Z.Y. Zhou, Y.S. Shen, DEM study of particle segregation in the throat region of a blast furnace, Powder Technol. 407 (2022) 117660, http://dx.doi.org/10.1016/j.powtec.2022.117660.

[10] W. Xu, S. Cheng, Q. Niu, W. Hu, J. Bang, The DEM study of segregation phenomena of burden distribution during the charging process of blast furnace with two parallel hoppers, Ironmak. Steelmak. 47 (2020) 337–343.

[11] Y. Yu, H. Saxén, Segregation behavior of particles in a top hopper of a blast furnace, Powder Technol. 262 (2014) 233–241, http://dx.doi.org/10.1016/j.powtec.2014.04.010.
[12] Y. Yu, H. Saxén, Particle flow and behavior at bell-less charging of the blast furnace, Steel Res. Int. 84 (2013) 1018–1033, http://dx.doi.org/10.1002/srin.201300028.
[13] M. Li, Y. Yu, H. Saxén, Numerical study on the behaviour and distribution of sinter during charging of a blast furnace with bell-less top, Miner. Eng. 228 (2025) 109365.
[14] H. Mio, M. Kadowaki, S. Matsuzaki, K. Kunitomo, Development of particle flow simulator in charging process of blast furnace by discrete element method, in: Minerals Engineering, vol. 33, 2012, pp. 27–33, http://dx.doi.org/10.1016/j.mineng.2012.01.002.
[15] H. Mio, S. Komatsuki, M. Akashi, A. Shimosaka, Y. Shirakawa, J. Hidaka, M. Kadowaki, S. Matsuzaki, K. Kunitomo, Validation of particle size segregation of sintered ore during flowing through laboratory-scale chute by discrete element method, ISIJ Int. 48 (2008) 1696–1703, http://dx.doi.org/10.2355/isijinternational.48.1696.
[16] H. Mio, S. Komatsuki, M. Akashi, A. Shimosaka, Y. Shirakawa, J. Hidaka, M. Kadowaki, S. Matsuzaki, K. Kunitomo, Effect of chute angle on charging behavior of sintered ore particles at bell-less type charging system of blast furnace by discrete element method, ISIJ Int. 49 (2009) 479–486, http://dx.doi.org/10.2355/ISIJINTERNATIONAL.49.479.
[17] H. Mio, S. Komatsuki, M. Akashi, A. Shimosaka, Y. Shirakawa, J. Hidaka, M. Kadowaki, H. Yokoyama, S. Matsuzaki, K. Kunitomo, Analysis of traveling behavior of nut coke particles in bell-type charging process of blast furnace by using discrete element method, ISIJ Int. 50 (2010) 1000–1009, http://dx.doi.org/10.2355/ISIJINTERNATIONAL.50.1000.
[18] T.F. Zhang, J.Q. Gan, A.B. Yu, D. Pinson, Z.Y. Zhou, Size segregation of granular materials during Paul-Wurth hopper charging and discharging process, Powder Technol. 378 (2021) 497–509, http://dx.doi.org/10.1016/j.powtec.2020.10.025.
[19] S. Wu, M. Kou, J. Xu, X. Guo, K. Du, W. Shen, J. Sun, DEM simulation of particle size segregation behavior during charging into and discharging from a paul-wurth type hopper, Chem. Eng. Sci. 99 (2013) 314–323, http://dx.doi.org/10.1016/j.ces.2013.06.018.
[20] J. Xu, Z. Hu, Y. Xu, D. Wang, L. Wen, C. Bai, Transient local segregation grids of binary size particles discharged from a wedge-shaped hopper, Powder Technol. 308 (2017) 273–289, http://dx.doi.org/10.1016/j.powtec.2016.12.013.
[21] J. Zhang, J. Qiu, H. Guo, S. Ren, H. Sun, G. Wang, Z. Gao, Simulation of particle flow in a bell-less type charging system of a blast furnace using the discrete element method, Particuology 16 (2014) 167–177, http://dx.doi.org/10.1016/j.partic.2014.01.003.
[22] W. Xu, S. Cheng, Q. Niu, W. Hu, J. Bang, Investigation on the uneven distribution of different types of ores in the hopper and stock surface during the charging process of blast furnace based on discrete element method, Met. Res. Technol. 116 (2019) http://dx.doi.org/10.1051/metal/2018099.
[23] D.K. Chibwe, G.M. Evans, E. Doroodchi, B.J. Monaghan, D.J. Pinson, S.J. Chew, Charge material distribution behaviour in blast furnace charging system, Powder Technol. 366 (2020) 22–35, http://dx.doi.org/10.1016/j.powtec.2020.02.048.
[24] S. Liu, Z. Zhou, K. Dong, A. Yu, D. Pinson, J. Tsalapatis, Numerical investigation of burden distribution in a blast furnace, Steel Res. Int. 86 (6) (2015) 651–661.
[25] T. Mitra, H. Saxén, Discrete element simulation of charging and mixed layer formation in the ironmaking blast furnace, Comput. Part. Mech. 3 (4) (2016) 541–555.
[26] H. Zhou, J. Wu, Z. Hong, L.P. Wang, S. Wu, M. Kou, G. Wang, Y. Luo, Numerical simulation of coke collapse and its optimization during burden charging at the top of bell-less blast furnace, Powder Technol. 389 (2021) 155–162.
[27] G. Degrassi, L. Parussini, M. Boscolo, N. Petronelli, V. Dimastromatteo, Discrete element simulation of the charge in the hopper of a blast furnace, calibrating the parameters through an optimization algorithm, SN Appl. Sci. 3 (2) (2021) 242.
[28] K. Zhou, Z. Jiang, D. Pan, W. Gui, J. Huang, Influence of charging parameters on the burden flow velocity and distribution on the blast furnace chute based on discrete element method, Steel Res. Int. 93 (1) (2022) 2100332.
[29] M. Kou, S. Wu, K. Du, W. Shen, J. Sun, Z. Zhang, DEM simulation of burden distribution in the upper part of COREX shaft furnace, ISIJ Int. 53 (2013) 1002–1009, http://dx.doi.org/10.2355/isijinternational.53.1002.
[30] M. Kou, J. Xu, H. Zhou, B. Wen, K. Gu, S. Yao, S. Wu, Effects of bottom base shapes on burden profiles and burden size distributions in the upper part of a COREX shaft furnace based on DEM, Adv. Powder Technol. 29 (2018) 1014–1024, http://dx.doi.org/10.1016/j.apt.2018.01.020.
[31] Z. Hong, H. Zhou, J. Wu, L. Zhan, Y. Fan, Z. Zhang, S. Wu, H. Xu, L.P. Wang, M. Kou, Effects of operational parameters on particle movement and distribution at the top of a bell-less blast furnace based on discrete element method, Steel Res. Int. 92 (2021) 2000262, http://dx.doi.org/10.1002/srin.202000262.
[32] M. Holmes, D. Penney, N. Lavery, S. Brown, A numerical investigation assessing the symmetry of burden charging in a blast furnace using different chute designs, Ironmak. Steelmak. 45 (6) (2018) 551–559.
[33] M. Kou, J. Xu, S. Wu, H. Zhou, K. Gu, S. Yao, B. Wen, Effect of cross-section shape of rotating chute on particle movement and distribution at the throat of a bell-less top blast furnace, Particuology 44 (2019) 194–206, http://dx.doi.org/10.1016/j.partic.2018.07.010.
[34] D. Schott, W. Vreeburg, C. Molhoek, G. Lodewijks, Granular flow to a blast iron ore furnace: Influence of particle size distribution on segregation of a mixture, in: Traffic and Granular Flow'15, Springer, 2016, pp. 621–628.
[35] P. Jacobs-Capdeville, S. Kuang, T. Evans, S. Song, A. Yu, GPU-DEM study of the flow and energy dissipation behaviors of burden materials in a full bell-less blast furnace charging system, Powder Technol. 459 (2025) 121035.
[36] H. Wei, C. Zhang, J. Han, Z. Wang, W. Ren, J. Zhang, Z. Chen, P. Lu, Effect of pellet proportion and charging sequence on burden distribution in blast furnaces according to discrete element method simulation, Processes 13 (1) (2025) 237.
[37] W. Zeng, D. Zou, G. Wang, W. Zheng, Y. Zhang, T. Zhang, H. Zhou, S. Wu, M. Kou, Particle size segregation during charging and discharging processes in bell-less blast furnace with serial-type hoppers, Steel Res. Int. 95 (12) (2024) 2400306.
[38] Z. Di, B. Yan, B. Cheng, S. Wang, C. Fan, Effects of particle size composition and burden ratio on burden segregation in the blast furnace throat based on DEM, Powder Technol. 448 (2024) 120319.
[39] L. He, X. Jiang, H. An, H. Zheng, Q. Gao, F. Shen, Effects of pellet ratio on the burden movement and distribution characteristics in the BF throat, Powder Technol. 432 (2024) http://dx.doi.org/10.1016/j.powtec.2023.119130.
[40] R. Roeplal, Y. Pang, A. Adema, J. van der Stel, D. Schott, Modelling of phenomena affecting blast furnace burden permeability using the discrete element method (DEM) – a review, Powder Technol. 415 (2023) http://dx.doi.org/10.1016/j.powtec.2022.118161.
[41] M. Geerdes, R. Chaigneau, O. Lingiardi, Modern Blast Furnace Ironmaking: an Introduction (2020), Ios Press, 2020.
[42] A. Hadi, R. Roeplal, Y. Pang, D.L. Schott, DEM modelling of segregation in granular materials: a review, KONA Powder Part. J. 41 (2024) 78–107.
[43] A. Hadi, Y. Pang, A. Adema, J. van der Stel, D. Schott, Insights into the segregation in the blast furnace charging system: from the stockhouse to top hoppers, La Met. Ital. (2024) 16.
[44] A. Hadi, Y. Pang, D. Schott, Systematic DEM calibration of two-component mixtures using AI-accelerated surrogate models, Powder Technol. (2025) 121190.
[45] H.P. Zhu, Z.Y. Zhou, R.Y. Yang, A.B. Yu, Discrete particle simulation of particulate systems: Theoretical developments, Chem. Eng. Sci. 62 (2007) 3378–3396, http://dx.doi.org/10.1016/j.ces.2006.12.089.
[46] J. Ai, J.-F. Chen, J.M. Rotter, J.Y. Ooi, Assessment of rolling resistance models in discrete element simulations, Powder Technol. 206 (2011) 269–282.
[47] A. Hadi, H. Shi, Y. Pang, D. Schott, Identification of dominant DEM parameters for multi-component segregation during heap formation, hopper discharge and chute flow, Powder Technol. 444 (2024) 119985.
[48] Delft High Performance Computing Centre (DHPC), DelftBlue supercomputer (phase 2), 2024, https://www.tudelft.nl/dhpc/ark:/44463/DelftBluePhase2.